Mutations in Subunits of the Activating Signal Cointegrator 1 Complex Are Associated with Prenatal Spinal Muscular Atrophy and Congenital Bone Fractures

Ellen Knierim,[1,2,13] Hiromi Hirata,[3,4,13,*] Nicole I. Wolf,[5] Susanne Morales-Gonzalez,[1,2] Gudrun Schottmann,[1,2] Yu Tanaka,[3] Sabine Rudnik-Schöneborn,[6,7] Mickael Orgeur,[8,12] Klaus Zerres,[6] Stefanie Vogt,[9] Anne van Riesen,[1] Esther Gill,[1,2] Franziska Seifert,[1,2] Angelika Zwirner,[1,2] Janbernd Kirschner,[10] Hans Hilmar Goebel,[11] Christoph Hübner,[1] Sigmar Stricker,[8,12] David Meierhofer,[8] Werner Stenzel,[11] and Markus Schuelke[1,2,*]

Transcriptional signal cointegrators associate with transcription factors or nuclear receptors and coregulate tissue-specific gene transcription. We report on recessive loss-of-function mutations in two genes (*TRIP4* and *ASCC1*) that encode subunits of the nuclear activating signal cointegrator 1 (ASC-1) complex. We used autozygosity mapping and whole-exome sequencing to search for pathogenic mutations in four families. Affected individuals presented with prenatal-onset spinal muscular atrophy (SMA), multiple congenital contractures (arthrogryposis multiplex congenita), respiratory distress, and congenital bone fractures. We identified homozygous and compound-heterozygous nonsense and frameshift *TRIP4* and *ASCC1* mutations that led to a truncation or the entire absence of the respective proteins and cosegregated with the disease phenotype. *Trip4* and *Ascc1* have identical expression patterns in 17.5-day-old mouse embryos with high expression levels in the spinal cord, brain, paraspinal ganglia, thyroid, and submandibular glands. Antisense morpholino-mediated knockdown of either *trip4* or *ascc1* in zebrafish disrupted the highly patterned and coordinated process of α-motoneuron outgrowth and formation of myotomes and neuromuscular junctions and led to a swimming defect in the larvae. Immunoprecipitation of the ASC-1 complex consistently copurified cysteine and glycine rich protein 1 (CSRP1), a transcriptional cofactor, which is known to be involved in spinal cord regeneration upon injury in adult zebrafish. *ASCC1* mutant fibroblasts downregulated genes associated with neurogenesis, neuronal migration, and pathfinding (*SERPINF1, DAB1, SEMA3D, SEMA3A*), as well as with bone development (*TNFRSF11B, RASSF2, STC1*). Our findings indicate that the dysfunction of a transcriptional coactivator complex can result in a clinical syndrome affecting the neuromuscular system.

Introduction

Arthrogryposis multiplex congenita (AMC) comprises a heterogeneous group of disorders that has a prevalence of 8.5/100,000 individuals and an incidence of 1/3,000–5,000 births and shares multiple congenital joint contractures as a defining feature.[1,2] AMC is caused by limited fetal movement (akinesia) resulting from conditions that impede intrauterine neuromuscular development.[3] Much has been learned from AMC-causing gene defects about the development of the human neuromuscular system. Mutations can affect the genes of structural proteins of the contractile apparatus,[4] trophic factors, proteins implicated in pathfinding[5,6] and myelination,[7] receptor proteins,[8,9] or proteins involved in transmitter release.[10]

In six out of seven individuals from our study, AMC occurred together with congenital bone fractures. From the epidemiologic view, congenital bone fractures are an extremely rare condition and are mainly due to trauma or osteogenesis imperfecta.[11] A retrospective birth register study of 343,941 newborns from Sweden uncovered 68 cases of multiple congenital contractures (incidence ~1/5,100). Of these 68 children, 14 had amyoplasia (incidence ~1/45,000), 18 had different neuromuscular disorders (incidence ~1/19,100), and only 2 had perinatal fractures (incidence ~1/172,000), although it was not mentioned to what group the latter two individuals belonged. Hall et al. analyzed the clinical symptoms of amyoplasia, the most frequent subform of AMC, and found a much higher frequency of congenital bone fractures among these children, in the range of ten percent.[12] Other rare disorders in which AMC associates with congenital bone fractures occur with mutations in *UBA1* (formerly *UBE1,* X-linked spinal muscular atrophy type 2 [SMAX2] [MIM: 301830]),[13,14] *FKBP10* (Bruck syndrome type 1 [MIM: 259450]),[15] and *ERBB3* (lethal congenital contracture syndrome type 2

[1]Department of Neuropediatrics, [2]NeuroCure Clinical Research Center
Charité Universitätsmedizin Berlin, 10117 Berlin, Germany; [3]Department of Chemistry and Biological Science, College of Science and Engineering, Aoyama Gakuin University, Sagamihara 252-5258, Japan; [4]Center for Frontier Research, National Institute of Genetics, Precursory Research for Embryonic Science and Technology, Japan Science and Technology Agency, Mishima 411-8540, Japan; [5]Department of Child Neurology, Neuroscience Campus Amsterdam, VU University Medical Center, 1007 MB Amsterdam, the Netherlands; [6]Institute of Human Genetics and University Hospital, Rheinisch-Westfälische Technische Hochschule Aachen University, 52074 Aachen, Germany; [7]Division of Human Genetics, Medical University Innsbruck, 6020 Innsbruck, Austria; [8]Max Planck Institute for Molecular Genetics, 14195 Berlin, Germany; [9]Medizinisches Versorgungszentrum Dr. Eberhard & Partner, 44137 Dortmund, Germany; [10]Department of Neuropediatrics and Muscle Disorders, University Medical Center Freiburg, 79106 Freiburg, Germany; [11]Department of Neuropathology, Charité Universitätsmedizin Berlin, 10117 Berlin, Germany; [12]Free University Berlin, Institute for Chemistry and Biochemistry, 14195 Berlin, Germany
[13]These authors contributed equally to this work
*Correspondence: hihirata@chem.aoyama.ac.jp (H.H.), markus.schuelke@charite.de (M.S.)
http://dx.doi.org/10.1016/j.ajhg.2016.01.006.

[LCCS2] [MIM: 607598])[16] and in several forms of nemaline myopathy.[17–19] Although the most severe form of infantile spinal muscular atrophy (SMA type 1, Werdnig Hoffmann disease [MIM: 253300]) is often associated with fetal akinesia, congenital bone fractures seem to be a rarity in this condition. In these children, fractures might occur later in life due to inactivity. We only found a single publication in which a case of SMA type 1 plus congenital bone fractures had been verified on the molecular level through detection of an *SMN1* deletion.[20] In most published cases of SMA plus congenital bone fractures, *SMN1* deletions had been excluded.[21–24] Hence, we set out to search for mutations in other genes that might involve neuromuscular development as well as bone metabolism in three families with six affected children who had AMC plus congenital fractures. Gene mapping and whole-exome sequencing (WES) revealed mutations in two genes that encode subunits of a transcriptional signal cointegrator complex.

Transcriptional signal cointegrators associate with transcription factors or with nuclear receptors in multi-protein complexes and are able to bi-directionally affect the link between receptor and transcription machinery, either as corepressors or coactivators. They enable the functional integration of multiple transcription factors[25] and thus fine-tune cell metabolism and transcription depending on environmental cues[26] or provide tissue specificity.[27] Over the past few years, a number of studies have shown that coactivator complexes are often bi-functional proteins that do not only coactivate transcription mediated by specific transcription factors, like nuclear hormone receptors, but also participate in pre-mRNA processing and regulation of splicing.[28] The tetrameric ASC-1 transcriptional cointegrator complex is composed of the following four subunits.[29] TRIP4 (thyroid receptor interacting protein 4 [MIM: 604501]) contains a conserved cysteine-rich Zn-chelating domain, which binds transcription factors,[29] and a conserved C-terminal domain, which harbors a RNA-binding PUA domain[30] thought to be an ancient structural motif for RNA-protein interactions. ASCC1 (ASC-1 complex, subunit 1 [MIM: 614215]) has an RNA-binding KH domain fused to a 2H RNA-phosphoesterase.[29,31] Not much is known about the ~100 kDa subunit ASCC2 (ASC-1 complex subunit 2 [MIM: 614216]). The largest subunit of ~200 kDa, ASCC3 (ASC-1 complex subunit 3 [MIM: 614217]), is an RNA helicase and shows paralogy to the small nuclear ribonucleoprotein 200, which is involved in RNA splicing. Hence, the ASC-1 complex is likely to be a ribonucleoprotein complex that participates in transcriptional coactivation, as well as in RNA processing events.

Methods

Ethics

Human samples were collected according to guidelines laid down in the Declaration of Helsinki in the amended version of 2013. All caretakers provided written informed consent for all investigations of the study (IRB approval of the Charité EA2/092/06). Zebrafish were raised and used in compliance with the guidelines approved by the animal care and use committee at the National Institute of Genetics (Japan).

Haplotype and Mutation Analysis

Autozygosity mapping[32] was performed with members of families A, B, and D (Figures S3–S5, members indicated by an asterisk on the pedigrees in Figure 2). WES was done in three index case individuals (B.II_01, D.II_02, D.II_03), as previously described.[33] DNA analyses were done with genomic DNA from blood leukocytes. For SNP analysis, we used the GeneChip Human Mapping 250K SNP Array (Affymetrix) and analyzed each separate family with the HomozygosityMapper software for autozygous regions that were only present in affected children and not in unaffected family members.[32]

For WES, we captured the exonic sequences by using the SeqCap EZ Human Exome Library v.3.0 (NimbleGen) and sequenced them on a HiSeq2000 (Illumina) machine. The paired-end reads were aligned to the 1000 Genomes GRCh37.p11 human reference sequence with the Burrows-Wheeler Aligner (BWA)-MEM v.0.7.1[34] and then fine-adjusted and called for deviations from the human reference with the Genome Analysis Toolkit (GATK) v.2.7 in all exonic ± 50 bp flanking regions.[35] For coverage details, see Table S2. The resulting variants were filtered for homozygosity (e.g., the absence of more than four homozygotes in the 1000 Genomes Project or of more than 20 homozygotes in the Exome Aggregation Consortium [ExAC] database) and the presence of the variant in the autozygous interval. These variants were then assessed by the MutationTaster software for potential pathogenicity.[36] Variants and their segregation were verified by bi-directional Sanger sequencing with the BigDye Terminator method (Applied Biosystems). Subsequently, we searched for *TRIP4* and *ASCC1* mutations in 11 unrelated children with AMC, respiratory distress, and congenital bone fractures by performing sequence analysis of the entire open reading frame and intron-exon borders of both genes; genomic primers are listed in Table S8.

Analysis of *TRIP4* Splice Isoforms

In order to explain the identity of the additional bands on the TRIP4 western blot, we used RT-PCR. mRNA from muscle tissue of affected children and control indiviuduals was reversely transcribed into cDNA and amplified with various primer combinations with forward primers (located at exons 1–5) and reverse primers (located at exons 8–13). Resulting PCR products were subcloned and subjected to bi-directional automatic Sanger sequencing. Resulting sequence fragments were aligned to the *TRIP4* reference sequence with the STAR v.2.4.0 software, which is able to identify novel splice junction sites.[5] For the identification of different splicing patterns in RNA-seq datasets from the GEO repository (Figure 3), we used the STAR v.2.4.0 aligner followed by analysis with the Cufflinks v.2.2.1 software suite.[37]

Histology

Cryosections from muscle biopsy specimens were stained with Gömöri trichrome, H&E non-specific esterase, and ATPases preincubated at pH 4.3, 4.6, and 9.4, as well as with primary antibodies directed against myosin heavy chain: MHC_{slow}, MHC_{fast}, MHC_{neo}, and MHC_{dev}. Signals were visualized with appropriate secondary antibodies and the diaminobenzidine system. Zebrafish

morphants were anesthetized at 48 hours post fertilization (hpf) in 0.02% tricaine (Sigma), fixed in cacodylate-buffered (pH 7.2) 2% glutaraldehyde, and prepared for electron microscopy as previously described.[38] The skeletal muscle was likewise processed for electron microscopy. For antibodies, see Table S9.

Western Blot

Western blot was performed with protein extracts from muscle and fibroblasts as previously described.[39] We used antibodies against TRIP4 and ASCC1. Anti-pan-Actin was used as loading control for muscle and β-tubulin for fibroblasts. Bands were visualized by chemiluminescence with peroxidase-labeled secondary antibodies. For antibodies, see Table S9.

Cell Sub-fractionation

Fibroblasts were yielded from nearly confluent plastic culture flasks by trypsination. Cross linking was done in DMEM with 1% formaldehyde for 10 min on ice. The reaction was stopped by adding glycine to a concentration of 130 mM, and the cells were spun down at 250 × *g* for 7 min. The pellet was resuspended in LF buffer (50 mM Tris-HCl [pH 7.5], 150 mM NaCl, 5 mM EDTA, 0.5% NP40, 1.15% Triton X-100, one Complete tablet [Roche]) and incubated for 10 min on ice. The cell suspension was then transferred into a Dounce tissue grinder where cells were broken by 10 up and down strokes and centrifuged for 10 min at 4°C at 3,000 × *g*. The supernatant was kept at −80°C as the cytosolic fraction. The pellet containing the nuclei was resuspended in freshly prepared nuclear lysis buffer (10 mM Tris-HCl [pH 8.0], 100 mM NaCl, 1 mM EDTA, 0.5 mM EGTA, 0.1% Na-deoxycholate, 0.5% N-lauroylsarcosine, one Complete tablet) and sonicated 10 times for 10 s on ice. Finally, a 1/10 volume of Triton X-100 was added and a centrifugation at 16,000 × *g* for 1 min was performed to remove debris. The supernatant was kept as the nuclear fraction.

Immunoprecipitation

500 μg protein of the nuclear fraction were mixed with 2 μg of specific antibody and incubated in 500 μl nuclear lysis buffer on a rotator at 4°C overnight. Washed 50 μl Protein-G Sepharose beads were then added and incubated on a rotator at 4°C overnight to let the beads bind to the specific antibodies. Beads were then spun down at 2,000 × *g* at 4°C for 2 min. The supernatant contained the unbound fraction. The bead pellet was then washed six times with wash buffer (50 mM HEPES-KOH [pH 7.55], 1 mM EDTA, 1.0% NP40, 0.7% Na-deoxycholate, 500 mM LiCl). For western blot, the beads were finally washed once with TE buffer (10 mM Tris-HCl [pH 8.0], 1 mM EDTA, 50 mM NaCl). Protein was eluted from the beads with elution buffer (50 mM Tris-HCl [pH 8.0], 10 mM EDTA, 1.0% SDS). Remaining beads were spun down at 2,000 × *g* at 4°C for 2 min, and the supernatant was used for SDS-PAGE. For mass spectrometry, the beads were finally washed once with 50 mM ammonium-bicarbonate (pH 8.0) and spun down at 2,000 × *g* for 2 min at 4°C. After removal of the supernatant, the pellets were frozen on dry ice.

Trip4 and *Ascc1* In Situ Expression Analysis in Mice and Zebrafish

Studies of *Trip4* and *Ascc1* gene expression were done in axial and sagittal sections of whole C57BL6/J mouse embryos (embryonic day 17.5 [E17.5]) by in situ hybridization as previously described.[40] Mouse embryos were embedded in TissueTek (Sakura), and longitudinal and axial sections were prepared on a cryostat. Riboprobes of ~600 bp length were generated by RT-PCR from mouse muscle with tailed primers (Table S8) and cloned into the pCR-Script vector (Clontech). After linearization of the vector, antisense and sense DIG-labeled probes were generated with T3 and T7 RNA polymerase (DIG RNA Labeling Kit, Roche), respectively. Hybridization was performed overnight at 60°C followed by a colorimetric reaction at room temperature (24–48 hr). Slides were photographed with a 20× lens on a DMI4000 (Leica) microscope. Single visual fields were joined by the tiling-software (Image-Pro Premier v.9.1) of the microscope to generate the cross-sectional image of the spinal cord and adjacent structures (Figure 4, Figures S6 and S7). Whole-mount in situ hybridization of zebrafish was performed as previously published,[6] with *trip4* and *ascc1* DIG-labeled antisense probes, and labeling with the respective sense probes did not detect any significant signal.

Functional Analysis in Zebrafish

MO-Mediated Knockdown of trip4 *and* ascc1

Two different antisense morpholino oligonucleotides (MOs) were designed against the splice acceptor sites of zebrafish *trip4* (boundary of intron 4 and exon 5) and *ascc1* (boundary of intron 3 and exon 4) (Figures S8–S10). These antisense MOs and a standard negative control MO were purchased from Gene Tools. The sequences of these MOs and the control MO are depicted on Table S8. Zebrafish embryos were injected with 5 ng of MOs at the one- or two-cell stage in three independent trials and studied as previously published.[6] At these dosages, the control MO produced no discernible phenotype change.

Quantification of MO-Mediated trip4 *and* assc1 *Knockdown on the mRNA Level*

Total RNA was extracted from a mixture of five MO-injected embryos and subjected to RT-PCR with the SuperScript III kit (Life Technologies) for reverse transcription. The number of reaction cycles for PCR was 23 for *trip4* and *ascc1* and 18 for *bactin*. All primer sequences are provided in Table S8. Quantitative analysis was done by measurement of band intensities of *trip4*, *ascc1*, and *bactin* with the ImageJ software, and p values were calculated with the t test.

Quantification of MO-Mediated trip4 *and* assc1 *Knockdown on the Protein and Morphological Levels*

For morphological analysis of α-motoneurons and neuromuscular junctions, zebrafish embryos (36 hpf) were anaesthetized in 0.02% tricaine (Sigma) and fixed in 4% paraformaldehyde (Sigma) at 4°C overnight and subjected to immunostaining as described previously (Figure 5).[6] The following antibodies and labeling reagents were used: anti-synaptotagmin (znp-1, 1:100), AlexaFluor488-conjugated anti-mouse immunoglobulin G (IgG, 1:1,000), and AlexaFluor594-conjugated α-bungarotoxin (1:1,000). Fluorescent images were captured with a confocal microscope (SP5, Leica). For antibodies, see Table S9. To quantify the reduction of neuromuscular junctions in the morphants, we densitometrically measured the intensities of the α-bungarotoxin staining in control and morphant zebrafish larvae by using ImageJ. Statistic analysis was done by t test.

Movement Analysis of Zebrafish

At 1 dpf, the chorion of the embryos was removed to allow touch access to the embryos. Embryos showing retarded development or developmental malformations, which were even seen in un-injected wild-type clutch, were removed before assay. Tactile stimulation was applied to the tail with a forceps (Movies S1, S2, and S3). Touch responses of MO-injected embryos (morphants) were video

recorded at 30 hpf with a high-speed camera at 200 frames per second (HAS-220, Ditect).[41] The normal touch response of control morphants at 1 dpf is a vigorous coiling behavior, twisting their tail to the trunk ("full coil"), but *ascc1* and *trip4* morphants displayed only a faint twitch without coiling their tail to the trunk ("partial coil"). The ratio of abnormal embryos showing partial coil to total embryos in the three experimental trials is provided in Table S3. Statistic analysis was done by the χ^2 test.

Rescue of MO-Knockdown with trip4 *and* ascc1 *Constructs*

Full-length zebrafish *trip4* and *ascc1* cDNAs were cloned into the pCS2+ zebrafish expression vector with the oligonucleotide primers detailed in Table S8. The *trip4* nonsense mutation leading to a truncation of the protein (zebrafish, p.Lys265*; corresponding alteration in humans, p.Arg278*) and the *ascc1* frameshift mutation, also leading to a truncation of the protein (zebrafish, p.Glu53Glyfs*) were introduced by site-directed mutagenesis. 100 pg of *trip4* or *ascc1* wild-type and mutant RNA were then injected into zebrafish embryos along with *trip4* or *ascc1* MOs, and the morphants were assayed for touch response and motoneuron and neuromuscular junction labeling (Figure S11, Table S5).

Cell Culture

Low passage skin fibroblasts of two affected children and four age-matched control individuals were grown to semi-confluency in DMEM supplemented with 15% fetal bovine serum (FBS) at 37°C in a 5% CO_2 atmosphere. After being washed with PBS, the cells were incubated with DMEM supplemented with 0.5% FBS over 24 hr for serum starvation. A fibroblast pellet was yielded after this period (time point = 00W). After being washed with PBS, the other culture dishes were incubated with DMEM supplemented with 15% FBS, and aliquots of cells were yielded exactly 30 min (time point = 30W) and 60 min (time point = 60W) later. All pellets were flash frozen in liquid nitrogen and stored at −80°C until further use.

Global mRNA Expression Profiling

Skin fibroblasts of affected children (D:II_2 and D:II_3) and of age-matched control indiviuduals (n = 4) were processed as described above. Total RNA was prepared from the frozen pellets with the standard TRIzol (Life Technologies) protocol. Quality of the RNA was controlled via the 2100 Bioanalyzer (Agilent). RNA was hybridized, according the manufacturer's instructions, on the GeneChip Human Gene 2.0 ST Array (Affymetrix), which represents 40,716 human RefSeq transcripts, including 30,654 transcripts which are annotated as protein coding. The chips were scanned with the 428 Scanner (Affymetrix) and data were processed with the Affymetrix GeneChip Command Console Software (AGCC) to produce the CEL files that could be uploaded to the GenePattern platform for further downstream analysis and visualization.[42] We first inspected those genes that are known downstream targets of serum response factor (SRF), which, however, failed to show any difference in serum-dependent regulation between affected children and control individuals (Figure S12). Next, we identified those genes that were significantly up- and downregulated in the samples from affected children in comparison to those from control individuals. In order to control for multiple testing, we only considered genes as significantly regulated if they had a false discovery rate (FDR) below 0.01. The raw data of this experiment can be accessed from the GEO database (GEO: GSE67627). Pathway and gene network analysis of the regulated genes was performed with AmiGO2.[43]

Statistics

For comparison of normally distributed values, we used the t test, and for not normally distributed values, either the χ^2 or the nonparametric Mann-Whitney U test. To control for multiple testing in the gene expression studies, we calculated the FDR,[44] and differences in gene expression were considered significant if the FDR was <0.01.

Results

Clinical Presentation in Eight Individuals from Four Families

We describe here a cohort of seven individuals who were born with distal and proximal joint contractures, as well as generalized muscle atrophy and fractures of their long bones (humerus and femur), and one aborted fetus. Deep tendon reflexes were absent, muscles did not contract upon electrical nerve stimulation, and neurography revealed axonal neuropathy in these indiviudals. Respiratory distress, diaphragmatic eventration and pulmonary hypoplasia necessitated mechanical ventilation soon after birth. Dysphagia required gavage feeding. For a detailed comparison of clinical symptoms, see Table 1. Most children died from respiratory failure between 2 weeks and 16 months of life. One child died from acute heart failure. Additional variable features included premature birth, microretrognathia, hypertelorism, a high-arched palate, secundum atrial septal defect, patent ductus arteriosus, and cardiomyopathy. In the affected children from family D, cerebral MRI had been performed and revealed a simplified gyral pattern of the cerebral cortex (Figure 1).

Muscle biopsy samples from four children were available for re-analysis (Figure 1): the muscle fibers were reduced in size, showed increased fiber-size variation, and were much more immature than samples from age-matched control individuals. The affected childrens' type I fibers were clustered in groups, in comparison to the checkerboard pattern in control individuals, which is a characteristic finding in prenatal SMA (Figure 1). In one individual, postmortem histology of the spinal cord was available and revealed numerous apoptotic α-motoneurons in the anterior horns at different levels (Figure 1). Sural nerve biopsy from two children showed normal density of myelinated fibers within the range of published reference values[46–48] (Figures S1 and S2, Table S1), but also showed signs of unmyelinated axon loss (Figure 1). The average axon diameters were increased in one individual from family B, but in the range of a normal age-matched control in an individual from family D (Figure S2). On X-ray, the bones of individual D.II_3 had failed to develop callus after 14 days of splinting. Subperiostal new bone formation would be expected after 11 days at the latest, and even earlier in young infants.[49] Bone mineralization and alkaline phosphatase activities were normal.

Autozygosity Mapping and WES

Even though families A and B denied consanguinity, we assumed a founder haplotype due to their common

Table 1. Clinical Data of the Investigated Families

	Family A	Family B	Family C	Family D	Total
Country of origin	Kosovo	Kosovo	Albania	Turkey	–
Gene involved	*TRIP4*	*TRIP4*	*TRIP4*	*ASCC1*	–
Mutation on the cDNA level	c.760C>T	c.832C>T	c.760C>T c.832C>T	c.157dupG	–
Predicted protein alteration	p.Arg254*	p.Arg278*	p.Arg254* p.Arg278*	p.Glu53Glyfs19*	–
Number of affected individuals	n = 2	n = 2 + (1)[a]	n = 1	n = 2	n = 7 + (1)[a]
Prenatal Manifestation: HPO ID					
Decreased or absent fetal movement: 1558	n = 2	n = 2	ND	n = 2	n = 6/6, 100%
Polyhydramnios: 1561	n = 0	n = 0	ND	n = 2	n = 2/6, 33%
Oligohydramnios: 1562	n = 2	n = 1	ND	n = 0	n = 3/6, 50%
Premature birth (< 37 weeks): 1622	n = 1	n = 1	ND	n = 2	n = 4/6, 67%
Nervous System: HPO ID					
Severe muscular hypotonia: 6829	n = 2	n = 2	n = 1	n = 2	n = 7/7, 100%
Areflexia: 1284	n = 2	ND	ND	n = 2	n = 4/4, 100%
Muscle weakness: 1324	n = 2	n = 2	ND	n = 2	n = 6/6, 100%
Global developmental delay: 1263	n = 2	n = 2	ND	n = 2	n = 6/6, 100%
Dysphagia: 2015	n = 2	n = 2	ND	n = 2	n = 6/6, 100%
Abnormal cortical gyration: 2536	ND	ND	ND	n = 2	n = 2/2, 100%
Head and Neck: HPO ID					
Microretrognathia: 0308	n = 2	n = 2	ND	n = 0	n = 4/6, 67%
Hypertelorism: 0316	n = 2	n = 1	ND	n = 0	n = 3/6, 50%
High palate: 0218	n = 2	n = 1	ND	n = 0	n = 3/6, 50%
Narrow mouth: 0160	n = 2	n = 0	ND	n = 0	n = 2/6, 33%
Cardiovascular System: HPO ID					
Patent foramen ovale: 1655	n = 0	n = 1	ND	n = 2	n = 3/6, 50%
Secundum atrial septal defect: 1684	n = 2	n = 0	ND	n = 0	n = 2/6, 33%
Patent ductus arteriosus: 1643	n = 2	n = 1	ND	n = 2	n = 5/6, 83%
Cardiac failure: 1635	n = 1	n = 0	ND	n = 0	n = 1/6, 17%
Cardiomyopathy: 1638	n = 1	n = 1	ND	n = 0	n = 2/6, 34%
Respiratory System: HPO ID					
Neonatal respiratory distress: 2643	n = 2	n = 2	n = 1	n = 2	n = 7/7, 100%
Pulmonary hypoplasia: 2089	n = 0	n = 2	ND	n = 2	n = 4/6, 67%
Musculo-skeletal System: HPO ID					
Multiple prenatal fractures: 5855	n = 2	n = 1	ND	n = 2	n = 5/6, 83%
Arthrogryposis multiplex congenita: 2804	n = 2	n = 3	n = 1	n = 2	n = 8/8, 100%
Muscle fiber immaturity: NA	n = 1	n = 2	ND	n = 1	n = 4/4, 100%
Muscle fiber size variation and atrophic fibers: 3557	n = 1	n = 2	ND	n = 1	n = 4/4, 100%

The families correspond to those in Figure 2. Abbreviations are as follows: HPO ID, Human Phenotype Ontology identifier; NA, not available; ND, not determined.[45]
[a]For Family B, the number in parentheses refers to an aborted fetus.

Kosovan origin and performed autozygosity mapping. Their shared autozygous region comprised 38 protein-coding genes (Figures S3–S5). Via WES of individual B.II_01, we found a homozygous nonsense mutation, c.832C>T (p.Arg278*), in *TRIP4* (chr15:64,701,816C>T [GRCh37], exon 7 [GenBank: NM_016213.4]). Genotype-phenotype

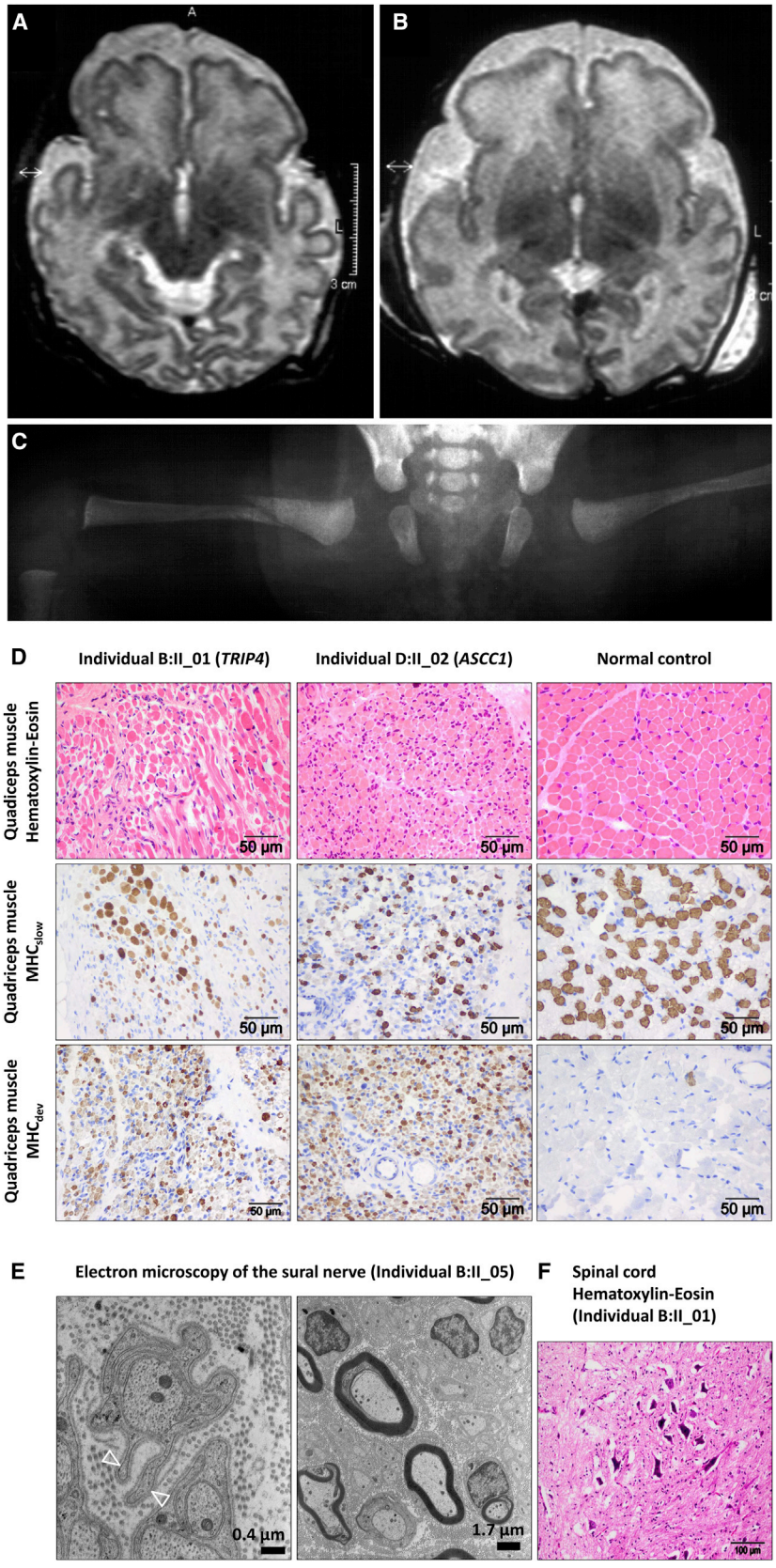

Figure 1. Clinical Presentation of the Affected Children

(A and B) Axial T_2-weighted cranial MRI images of affected children D.II_02 (A) (at a corrected gestational age of 39 weeks) and D.II_03 (B) (at a corrected gestational age of 37 weeks) with a simplified gyral pattern of the frontal lobes and enlargement of the external CSF spaces. Myelination of the brain stem and the basal ganglia is normal.

(C) X-ray of the bilateral congenital femoral fractures of individual D.II_03.

(D) Muscle histology demonstrates a reduction in fiber size and an increase in fiber-size variation in two individuals with a *TRIP4* and *ASCC1* mutation, in contrast to fiber size and variation in an age-matched control individual. The grouping of the larger type I fibers (marked by MHC_{slow}), in contrast to a normal checkerboard pattern in the control individual, is characteristic for prenatal SMA. The intense staining of the muscles of the affected children for MHC_{dev} highlights their immaturity.

(E) Ultrastructure of a sural nerve biopsy specimen with normal myelinization but with loss of unmyelinated axons as documented by "empty" pouches (open triangles).

(F) Presence of multiple intensely stained apoptotic α-motoneurons in the anterior horn of the spinal cord in a postmortem sample.

segregation was verified by Sanger sequencing of the entire family, including DNA from a fetus, who had been aborted at 27 weeks and 3 days, after joint contractures were observed on ultrasound imaging (Figure 2). Sequencing of *TRIP4* in family A also revealed a nonsense mutation (c.760C>T [p.Arg254*]), albeit unexpectedly, at a different position (chr15: 64,698,591C>T [GRCh37], exon 6), and homozygosity of this mutation segregated with the disease. Both mutations were absent in the 1000 Genomes Project as well as in 135 ancestry-matched in-house exomes. The p.Arg278* truncation was present in heterozygous form in 2/121,356 alleles of the ExAC database (accessed November 2015), in two individuals of European and African descent, whereas the p.Arg254* truncation was not listed.

Despite a similar clinical phenotype, autozygosity mapping located the disease locus of family D not on chr15, but on chr10. Using WES, we discovered a frameshift mutation, c.157dup (p.Glu53Glyfs*19), in *ASCC1* (chr10:73,970,544_5insC [GRCh37], exon 3 of ASCC1-003 [Ensembl: ENST00000317168] [GenBank: NM_001198800.2]) that was homozygous only in the affected children (Figure 2). This mutation is present in heterozygous form in 2/120,662 alleles of the ExAC database, in

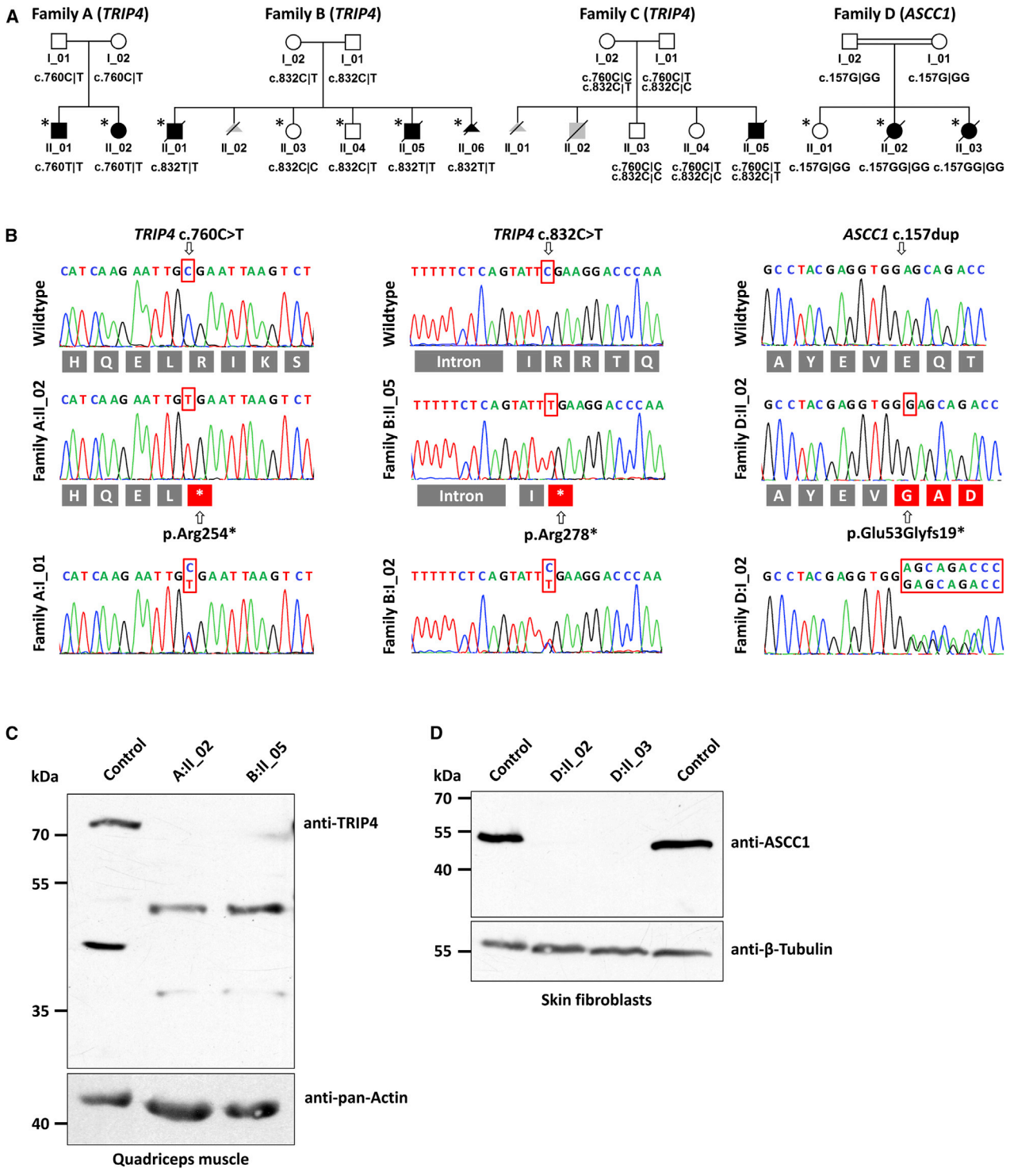

Figure 2. Pedigrees of the Families and Molecular Genetic Findings

(A) The pedigrees of all investigated families with their respective genotypes are depicted below the symbols. Individuals marked with an asterisk were used for autozygosity mapping.

(B) Variants identified by WES were verified by Sanger sequencing for segregation in all family members. Below the electropherograms, the reading frame of the respective amino acids is provided in the three letter code. Both *TRIP4* mutations resulted in a premature termination codon, whereas the *ASCC1* mutation led to a frameshift with a termination codon after insertion of 19 non-original amino acids.

(C) Western blot of a muscle protein extract from two individuals with a *TRIP4* mutation and from a control individual. The premature termination codons in both affected children lead to upregulation of an alternative splice isoform at ~53 kDa that excludes both mutant positions. Anti-pan-Actin band density was used as a loading control.

(D) Western blot of a protein extract from cultured fibroblasts of both children from family D and of two control individuals. The blot demonstrates the complete absence of the ASCC1 band in the affected children. β-tubulin band density was used as a loading control.

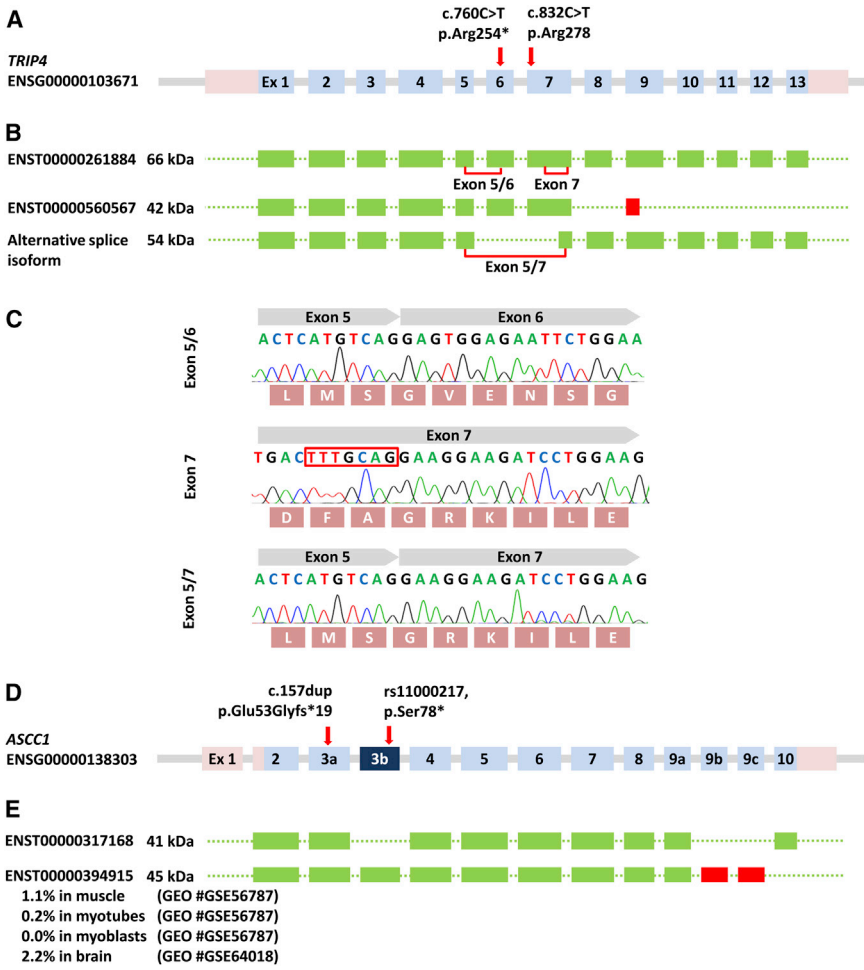

Figure 3. Splice Isoforms of *TRIP4* and *ASCC1*

(A) Genomic structure of *TRIP4* (not drawn to scale). The introns are indicated by gray lines.

(B) The exons included into the various mRNA splice isoforms are depicted in green, and the red box indicates a frame-shift.

(C) Sequence traces of the exon splice junctions. Their respective localization is marked on (B). The alternative splice acceptor site in exon 7 is highlighted by a red box.

(D) Genomic structure of *ASCC1* (not drawn to scale).

(E) The transcript encoding the 41 kDa ASCC1 is the most abundant. Exon 3b, which contains a missense mutation in 5.4% of the ExAC alleles and leads to the truncation of the protein (p.Ser78*), is only present in a rare ASCC1 45 kDa splice variant found in 0%–2% of the indicated GEO RNA-seq datasets.

two individuals of European and Latino descent. Interestingly, the ExAC database lists a variant in *ASCC1* (rs11000217) in 896/16,490 alleles (59 of them homozygotes), mainly in individuals from African or South Asian descent, that causes a truncation of ASCC1 (p.Ser78*). Such a finding might put into question the essential importance of ASCC1 for the ASC-1 complex. However, a transcriptomic analysis of RNA-seq datasets from muscle and brain revealed that this variant (dbSNP: rs11000217) resides in an exon that is only included in 0%–2% of the transcripts from the *ASCC1* locus (exon 3b, Figure 3), whereas the exon 3a that carries the mutation of the affected children in our study is present in >95% of the transcripts.

Cohort screening of *TRIP4* and *ASCC1* in 11 unrelated affected children with the appropriate phenotype revealed an additional individual (C:II_05), who also originated from the Balkans (Albania) and carried both *TRIP4* mutations in compound heterozygous state (Figure 2).

In order to further exclude mutations in other (known) genes that might have an influence on the phenotype of our affected children, we specifically searched within the autozygous regions of families A, B, and D for variants in genes that were associated in the Human Phenotype Ontology[45] with "arthrogryposis, HP:0002804," "fractures, HP:0003084," "spinal muscular atrophy, HP:0007269," "muscle weakness, HP:0001324," or with "abnormity of cortical gyration, HP:0002536," but did not find any other potentially pathogenic variants, either in heterozygous or in homozygous states.

Given that cryo-muscle samples were available from individuals A:II_02 and B:II_05, we studied the effect of the mutation on the protein level by western blot. Whereas, in normal muscle, we found two bands at ~40 and ~70 kDa and an additional very weak band at ~53 kDa, both individuals exhibited bands at ~53 kDa and ~36 kDa, with absence of the ~40 kDa and ~70 kDa bands (Figure 2). Interestingly, both mutant TRIP4 bands migrated at the same molecular size despite the fact that the premature termination codons were located at different positions. RT-PCR analysis of different *TRIP4* splice isoforms (Figure 3) revealed the activation of a cryptic splice acceptor site leading to a novel isoform with skipping of exons 6 and part of exon 7 that preserved the reading frame but excluded both missense mutations. This splice isoform seems to be upregulated in mutant cells, whereas the full-length transcript was subjected to nonsense mediated messenger decay. Such corrective splicing events leading to the upregulation of a rare splice isoform have been described, albeit rarely, for other conditions, such as spinal muscular atrophy (MIM: 253300),[50] Rothmund-Thomson syndrome (MIM: 268400),[51] retinitis pigmentosa (MIM: 304020),[52] Ullrich congenital muscular dystrophy (MIM: 254090),[53] and epidermolysis bullosa (MIM: 226650).[54] In these reported cases, the truncated proteins were expressed and seemed to retain some residual function that ameliorated the clinical phenotype. From family D, we only had cultured fibroblasts, which entirely

lacked ASCC1 and in which we did not detect any corrective splice isoforms that excluded the mutant exon (Figure 2).

Subcellular Location of the ASC-1 Complex

TRIP4 had been shown previously by indirect immunofluorescence to be a nuclear protein that localized into the cytoplasm under conditions of serum deprivation.[55] Because TRIP4 forms a tetrameric protein complex, we hypothesized that its correct subcellular localization might be compromised if one subunit (e.g., TRIP4 or ASCC1) of the ASC-1 complex was altered. Hence, we separated nuclear and cytosolic fractions of wild-type and *ASCC1* mutant fibroblasts under normal growth conditions, after serum depletion, and after serum depletion with subsequent 30 and 60 min of serum re-challenge and probed them on western blot with antibodies directed against three subunits of the ASC-1 complex (anti-TRIP4, anti-ASCC1, anti-ASCC2). We were unable to confirm a translocation to the cytoplasm under serum starvation, neither of the entire ASC-1 complex nor of TRIP4 alone. The signals of three subunits of the ASC-1 complex remained stationary in the nuclear fraction independently of the presence or absence of serum (Figure S13).

Trip4 and *Ascc1* Expression Analysis in Mouse Embryos by In Situ Hybridization

To determine the spatial expression pattern of *Trip4* and *Ascc1* in a later phase of embryonic development, we performed in situ hybridization on cryosections of E17.5 mouse embryos. Both genes showed nearly identical mRNA-expression patterns with ubiquitous expression, albeit at different levels (Figure 4). Highest expression was seen in dorsal root ganglia, the paraspinal sympathetic and trigeminal ganglia, and thyroid and submandibular glands, as well as the spinal cord. Expression in the cerebral cortex was comparable to the expression in the spinal cord.

MO Knockdown of *trip4* and *ascc1* in Zebrafish

The function of TRIP4 and ASCC1 in vertebrates has not been explored. To evaluate the physiological consequences of the absence of both mutant proteins, we performed a MO-mediated knockdown of *trip4* and *ascc1* in zebrafish, given that both proteins are conserved between humans and zebrafish (Figures S14 and S15). Based on the postmortem findings regarding the affected children, which revealed numerous apoptotic neurons in the anterior horn of the spinal cord, and the muscle histology of prenatal SMA, we focused our investigation on α-motoneuron and muscle development. Indeed, we found a severe impairment of axonal outgrowth, formation of the neuromuscular junction, and organization of the myotome (Figure 5, Table S3). Control MO-injected embryos responded to touch with typical coiling behavior, which consists of two to three vigorous contractions of trunk and tail at 30 hpf.[41] Knockdown of *trip4* or *ascc1* resulted in a compromised response (Movies S1, S2, and S3, Table S3). The knockout coiling phenotype of zebrafish could be rescued by injection of the respective full-length wild-type *trip4* and *ascc1* mRNA, but not by injection of mRNA carrying the affected childrens' mutations (Figure S11). To verify the specificity of the used MO, we used a second MO (MO2) aimed at a different splice site and were able to reproduce the original effect (Figure S10, Table S4). These loss-of-function analyses confirm that *trip4* and *ascc1* are indispensable for motor system development. In accordance with the observation of the motor behavior, the myotomes, as well as the neuromuscular endplates, appeared severely disorganized on electron microscopy (Figure 5).

Identification of ASC-1 Target Genes

In order to identify those genes whose mRNA transcript levels are differently regulated in the absence of a functionally intact ASC-1 complex, we performed a global mRNA expression analysis of *ASCC1* mutant and control fibroblasts after serum depletion and re-challenge (Figure 6, Table S6). Contrary to the originally published hypothesis that the ASC-1 complex might regulate transcription via the SRF,[29] we discovered normal upregulation of the SRF-dependent downstream target genes *FOS* (MIM: 164810), *IER2, FOSL1* (MIM: 1365150), *FOSB* (MIM: 164772), *JUNB* (MIM: 165161), and *TRIB1* (MIM: 609461) after serum challenge that was indistinguishable between affected and control fibroblasts (Figure S12). Hypothesis-free analysis of expression patterns after stringent filtering against genes with a FDR >0.01 revealed downregulation of 44 genes (Figure 6, Table S6), 13 of which are involved in neurogenesis (*SERPINF1* [MIM: 172860], *NOV* [MIM: 164958]), neuronal projection (*SERPINF1, CRABP2* [MIM: 180231]), pathfinding (*SEMA3A* [MIM: 603961], *SEMA3D* [MIM: 609907]), migration (*DAB1* [MIM: 603448]), and suppression of neuronal apoptosis (*SERPINF1, CRLF1* [MIM: 604237]). On the other hand, genes that suppress neuronal plasticity (*HAPLN1* [MIM: 115435]) and negatively regulate neuron projection (*CDH13* [MIM: 601364]) were upregulated. Six of the downregulated genes (Figure 6, Table S6) are involved in the negative regulation of bone resorption (*TNFRSF11B* [MIM: 602643]), ossification and regulation of osteoblast differentiation (*RASSF2* [MIM: 609492]), and collagen fibril organization (*DPT* [MIM: 125597]), as well as calcium ion homeostasis (*FAM20A* [MIM: 611062], *STC1* [MIM: 601185]).

Identification of ASC-1 Binding Partners

Immunoprecipitation with three different antibodies (anti-TRIP4, anti-ASCC1, and anti-ASCC2) against subunits of the ASC-1 complex mutually copurified the other members of the holocomplex (Figures 7 and S16–S18, Table S7). Even in the absence of ASCC1, copurification between TRIP4 and ASCC2 was still possible (Figures S16 and S18), suggesting the stability of the complex even in the absence of one subunit. Mass spectrometric analysis of the immunoprecipitates consistently identified copurification of the cysteine and glycine rich protein 1 (CSRP1), a transcriptional cofactor that is known to be involved in

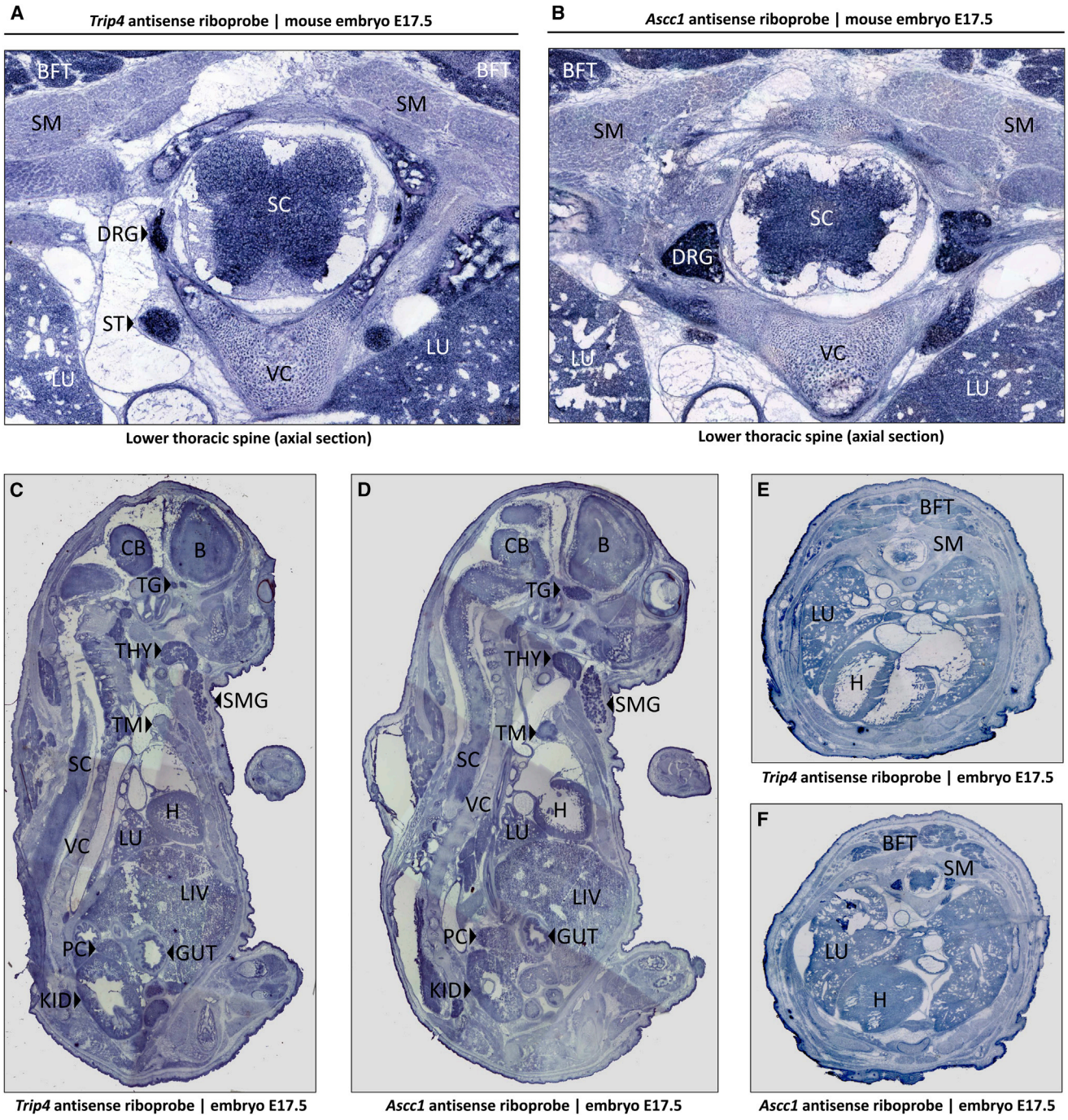

Figure 4. Gene Expression Study in E17.5 Mouse Embryos
In situ hybridizations of cryosections from E17.5 mouse embryos demonstrate the nearly identical expression patterns of *Trip4* (A, C, and E) and of *Ascc1* (B, D, and F) mRNA. At the lower thoracic level (A and B), the highest expression levels were seen in the spinal cord, dorsal root ganglia, paraspinal sympathetic ganglia, muscle, lung, and brown fat tissue. In the parasagittal sections, the highest expression levels were seen on the thyroid and submandibular salivary gland and the trigeminal ganglion. Abbreviations are as follows: B, brain; BFT, brown fat tissue; CB, cerebellum; DRG, dorsal root ganglion; GUT, gut; H, heart; KID, kidney; LIV, liver; LU, lung; PC, pancreas; SC, spinal cord; SM, skeletal muscle; SMG, submandibular salivary gland; ST, sympathetic tract; TG, trigeminal ganglion; TG, thyroid gland; TM; thymus; VC, vertebral column.

spinal cord regeneration in adult zebrafish (Table S7, Figures S19–S23).[56] Copurification of the CSRP1 protein was additionally verified by western blot of all three anti-ASC-1 immunoprecipitates with an anti-CSRP1 antibody (Figure 7).

Discussion

Our data show that mutations in two genes that encode different subunits (TRIP4 and ASCC1) of the activating signal cointegrator 1 (ASC-1) complex cause a profound

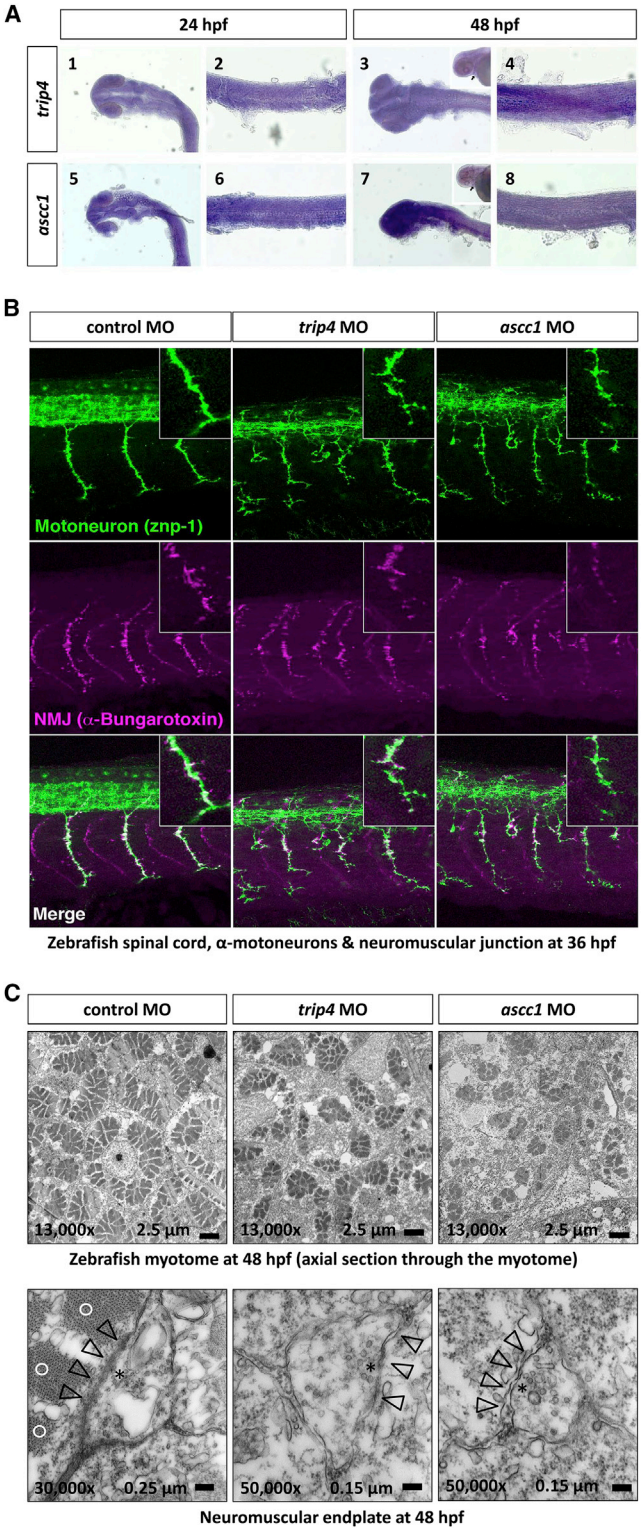

Figure 5. Studies on Zebrafish Embryos

Expression of *trip4* and *ascc1* mRNA.

(A) *trip4* is expressed ubiquitously in the head (A1) and trunk (A2) at 24 hpf and at 48 hpf (A3 and A4). *ascc1* is also expressed ubiquitously in the head (A5) and trunk (A6) at 24 hpf and 48 hpf (A7 and A8). The arrowheads indicate the heart, verifying that both *trip4* and *ascc1* are expressed in cardiac muscles.

(B) MO-mediated *trip4* and *ascc1* knockdown in zebrafish larvae led to a severe derangement of α-motoneuron axons and the myotome. In the morphants, we found a perturbed outgrowth of α-motoneuron axons projecting to the trunk muscle in every somite segment at 36 hpf. The α-motoneurons were short, thin, and fragile with abnormal branches in *trip4* morphants and *ascc1* morphants. In these morphants, we additionally see ectopic outgrowth of motoneurons from the spinal cord. The α-motoneurons are labeled with the znp-1 antibody (green). Labeling with α-bungarotoxin (purple) displays the formation of neuromuscular junctions that form along with the α-motoneurons. The neuromuscular junctions were thin, reduced in number, and disorganized in the *trip4* and *ascc1* morphants.

(C) Electron-microscopic images of axial sections through the zebrafish myotome at 48 hpf. The rosette-like formation of myofibrils is greatly disturbed with reduced size and numbers. The lower panels show a neuromuscular endplate of the control morphants (left) with a normal thickened basal lamina, which is directly adjacent to the contractile elements of the myofibril. This is in contrast to the endplates from the *trip4* and *ascc1* morphants, which are smaller and have a disrupted basal lamina and no adjacent contractile elements. An asterisk denotes clusters of neurotransmitter vesicles (vesicle diameter 30–40 nm); open arrowheads denote the synaptic cleft and basal lamina of the neuromuscular endplate; open circles denote sarcomers (contractile elements) in the vicinity of the neuromuscular endplate. Note the higher magnification of the morphant endplate.

disturbance of neuromotor unit development and result in prenatal onset spinal muscular atrophy with bone fractures. The notion that these two proteins form a functional complex and are involved in the same biological process in vivo is supported (1) by the nearly identical mRNA-expression pattern in the mouse embryo, (2) by the indistinguishable phenotypes of *trip4* and *ascc1* zebrafish morphants, (3) by mutual coimmunoprecipitation, and (4) ultimately by the similar phenotype of affected children and zebrafish. Such a phenomenon is known for other genetic disorders, such as leukoencephalopathy with vanishing white matter, which can be caused by alterations in five different subunits of the translation initiation factor eIF2B.[57]

The ASC-1 complex is composed of four subunits, which bind to nuclear receptors and coactivate the transcription of a wide range of transcripts. One subunit, TRIP4, was initially identified as a transcriptional coactivator of the thyroid hormone receptor.[58] Later, it was shown that TRIP4 stably associates with three other polypeptides, the activating signal cointegrator subunits 1–3 (ASCC1–ASCC3), and interacts with a wider range of transcription factors such as activating protein 1 (AP-1), nuclear factor kappa-B (NF-κB), and SRF.[29] In particular, the latter interaction between TRIP4 and SRF, which had been demonstrated by reporter gene assays,[29] seemed to offer a functional link between genetic defect and disease phenotype because SRF is an essential transcription factor for muscle,[59] nervous system,[60,61] and bone[62] development. However, we detected neither physical interaction between SRF and ASC-1 (Figures S16–S18) nor abnormal SRF-dependent transcription of downstream target genes in affected childrens' fibroblasts after serum depletion and re-challenge (Figure S12).

To explore alternative explanations for the pathomechanism seen in the affected children studied here and to

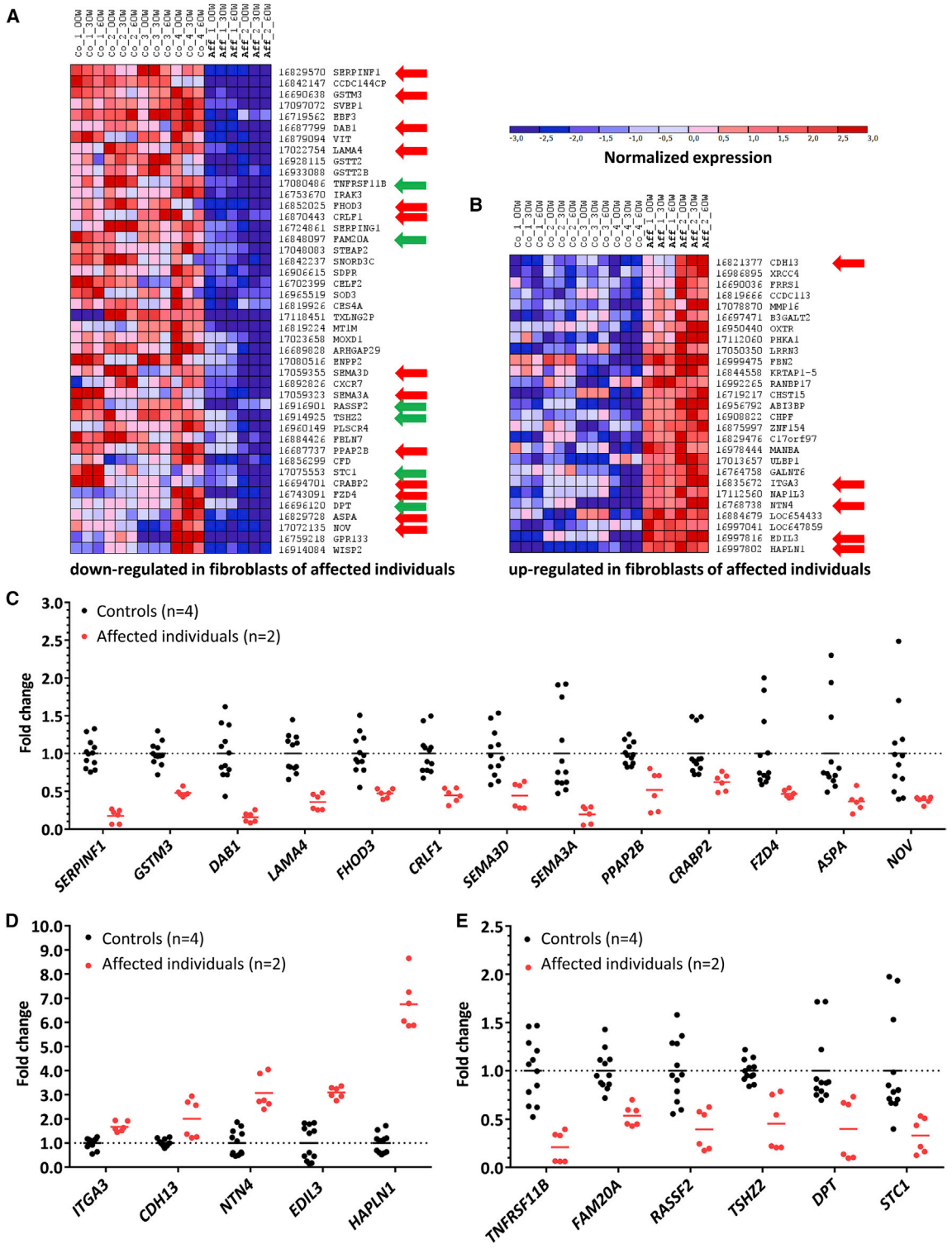

Figure 6. Gene Expression Analysis of Wild-Type and *ASCC1* Mutant Fibroblasts

(A) Clustergram of genes downregulated in fibroblasts of affected children with FDR < 0.01. Blue denotes normalized downregulation; red denotes upregulation (see attached scale above). The numbers on the right identify the Affymetrix Human GeneChip 2.0 probe set. The gene names are given on the far right column. The red arrows depict genes involved in neurogenesis; green arrows depict genes involved in bone metabolism. Abbreviations are as follows: Co, control; Aff, affected individual with *ASCC1* mutation; 00W, serum starved for 12 hr; 30W, serum challenge for 30 min; 60W, serum challenge for 60 min; FDR, false discovery rate.

(B) Genes upregulated in fibroblasts of affected children with FDR < 0.01.

(C and D) Genes involved in neurogenesis that are downregulated (C) or upregulated (D) in *ASCC1* mutant fibroblasts (red dots).

(E) Downregulated genes involved in bone metabolism and development (red dots). Each dot represents a separate hybridization experiment. Black dots denote control individuals; red dots denote affected individuals. The horizontal lines represent the arithmetic mean.

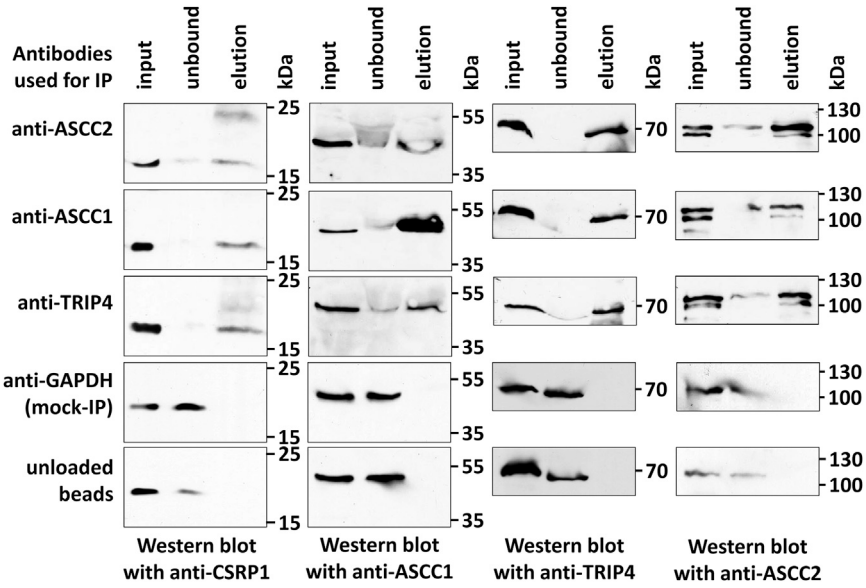

Figure 7. Coimmunoprecipitation of CSRP1 with Three Subunits of the ASC-1 Complex

Immunoprecipitation was done with anti-TRIP4, anti-ASCC1, and anti-ASCC2 antibodies. For mock immunoprecipitation, we used GAPDH antibodies, and for empty controls, we used unloaded Protein-G-Sepharose beads. Western blots from input, flow-through (unbound), and bound protein (elution) were serially incubated with anti-TRIP4, anti-ASCC1, anti-ASCC2, as well as with anti-CSRP1 antibodies.

search for proteins that bind to ASC-1, we performed an immunoprecipitation of the ASC-1 complex in fibroblasts of affected children and controls. Using mass spectrometry analysis, as well as western blot after immunoprecipitation, we consistently found coimmunopurification of CSRP1. CSRP1 localizes to the nucleus in the same manner as the ASC-1 complex (Figure S13).

CSRP1 is an evolutionarily highly conserved 23.4 kDa transcriptional coactivator that shares 83% identity between humans and zebrafish on the amino acid level. It contains a double zinc-finger motif, a nuclear localization signal, and a LIM motif, suggesting its involvement in developmental processes.[63,64] In the E14.5 mouse embryo, strong expression can be found in the CNS, especially in the spinal cord.[65] MO-mediated knockdown of *csrp1* in zebrafish during early development resulted in abnormal axis formation and severe deformities of midline structures. Miyasaka et al. also demonstrated that Csrp1 interacts with dishevelled 2 and diversin, thereby controlling cell morphology and the generation of pseudopodial processes via the non-canonical Wnt and JNK pathways.[66] Both pathways largely influence the generation of filopodia at axonal growth cones and are deemed essential for neuronal polarity and axon outgrowth and branching, as well as the navigation to their final targets. Interestingly, in adult zebrafish, which have the capability to regrow severed descending spinal axons after spinal injury and regain locomotor activity, Ma et al.[56] demonstrate a direct influence of Csrp1 on the re-growth behavior of axons. In contrast to mammals, zebrafish are able to reactivate specific developmental programs for regenerative purposes, and Ma et al. found a significant upregulation of *csrp1* in those neurons that regrew their axons, whereas MO-mediated *csrp1* knockdown impaired axonal regeneration and subsequent locomotor recovery.

We are aware that the conjectures about ASC-1 and CSRP1 interaction have to be proven in a mammalian system. It would thus be an interesting line of research to investigate how the simultaneous presence of ASC-1 and CSRP1 would shape neuronal patterning, outgrowth, pathfinding, and endplate formation. Because a complete knockout of *Csrp1* would most likely be embryonically lethal,[66] such experiments would have to be done in conditional knockout mice and with an α-motoneuron specific Cre-driver line.

Comparison of gene expression between mutant and wild-type cells shows that the ASC-1 complex exerts an influence on entire modules of genes (Figure 6, Table S6), many of which either enhance neurodevelopment and pathfinding or whose products suppress other genes that negatively regulate neuron projection, cell proliferation, or neuronal plasticity. Despite the fact that the mRNA expression analyses could only be done in the available fibroblasts of the affected children, it has been shown for another disease (MCT8-deficiency) that analysis of genome-wide expression data from fibroblasts derived from affected individuals was able to identify the dysregulation of coexpressed gene modules[67] that are disease specific and mirror those seen in the human brain transcriptome.[68]

As an example from our cohort, *SERPINF1* (serum peptidase inhibitor F), the most prominently downregulated gene (−5.7-fold) in mutant fibroblasts, has been shown to be involved in the positive regulation of spinal axon sprouting,[69] neuroprotection,[70] and survival of spinal motoneurons,[71] whereas the extracellular matrix protein *HAPLN1* (hyaluronan and proteoglycan link protein), the most prominently upregulated gene (+6.7-fold) in mutant fibroblasts suppresses neuronal plasticity.[72] The same modular phenomenon can be seen for genes involved in bone development. Here, the *TNFRSF11B* (tumor necrosis factor receptor superfamily, member 11b; osteoprotegerin) gene was most prominently downregulated (−4.8-fold). Osteoprotegerin functions as an inhibitor of osteoclastogenesis[73] and bone resorption[74] and positively regulates bone mass.[75]

In conclusion, the ASC-1 complex seems to be involved in the highly regulated development of the neuromuscular

unit and possibly of the neighboring bony structures as well. However, further research is needed to elucidate the exact signaling pathways that are involved in the patterning and development of the neuromuscular unit via the ASC-1 complex. Knowledge about the factors involved might have implications for regenerative medicine.

Accession Numbers

Raw data from the gene expression analysis of *ASCC1* mutant versus control fibroblasts can be accessed under the accession number GEO: GSE67627.

Supplemental Data

Supplemental Data include 23 figures, 9 tables, and 3 movies and can be found with this article online at http://dx.doi.org/10.1016/j.ajhg.2016.01.006.

Acknowledgments

We thank the parents and their children for participation at this study, Hannah Plückhan for excellent technical assistance in electron microscopy, and Beata Lukaszewska-McGreal for LC-MS/MS sample preparation. The project was funded by grants from the Deutsche Forschungsgemeinschaft (DFG; SFB 665 TP C4) and the Einstein Foundation Berlin (A-2011-63) to M.S., the Grant-in-Aid for Scientific Research (25920008) of the Ministry of Education, Culture, Sports, Science, and Technology of Japan and funding from the Takeda Science Foundation, the Mochida Memorial Foundation for Medical and Pharmaceutical Research, the Naito Foundation, and the Suzuken Memorial Foundation to H.H., by DFG (Ru746/1-2) and Interdisziplinäres Zentrum für Klinische Forschung Aachen (NP 5-4) grants to S.R.S., and by funding from the Planck Institute for Molecular Genetics to D.M. Additionally, M.S. is member of the NeuroCure Center of Excellence (grant no. Exc 257).

Received: September 18, 2015
Accepted: January 5, 2016
Published: February 25, 2016

Web Resources

The URLs for data presented herein are as follows:

1000 Genomes, http://browser.1000genomes.org
1000 Genomes reference sequence, ftp://ftp.1000genomes.ebi.ac.uk/vol1/ftp/technical/reference/human_g1k_v37.fasta.gz
AmiGO2, http://amigo2.berkeleybop.org/amigo/
BLAST, http://blast.ncbi.nlm.nih.gov/Blast.cgi
CRAPome database, http://www.crapome.org
Cufflinks v.2.2.0 software, http://cole-trapnell-lab.github.io/cufflinks/
dbSNP, http://www.ncbi.nlm.nih.gov/projects/SNP/
Ensembl Genome Browser, human genome, http://useast.ensembl.org/Homo_sapiens/Info/Index
ExAC Browser, http://exac.broadinstitute.org/
GATK, https://www.broadinstitute.org/gatk/
GenePattern, http://genepattern.broadinstitute.org/gp/pages/login.jsf
GEO, http://www.ncbi.nlm.nih.gov/geo/
HomozygosityMapper software, http://www.homozygositymapper.org/
Mouse Genome Informatics, http://www.informatics.jax.org/image/MGI:5329998
MutationTaster, http://www.mutationtaster.org/StartQueryEngine.html
OMIM, http://www.omim.org/
RefSeq, http://www.ncbi.nlm.nih.gov/RefSeq
STAR v.2.4.0 software, https://code.google.com/archive/p/rna-star/
T-Coffee, http://tcoffee.crg.cat/

References

1. Hoff, J.M., Loane, M., Gilhus, N.E., Rasmussen, S., and Dalt-veit, A.K. (2011). Arthrogryposis multiplexa congenita: an epidemiologic study of nearly 9 million births in 24 EUROCAT registers. Eur. J. Obstet. Gynecol. Reprod. Biol. *159*, 347–350.
2. Hall, J.G. (2014). Arthrogryposis (multiple congenital contractures): diagnostic approach to etiology, classification, genetics, and general principles. Eur. J. Med. Genet. *57*, 464–472.
3. Bamshad, M., Van Heest, A.E., and Pleasure, D. (2009). Arthrogryposis: a review and update. J. Bone Joint Surg. Am. *91* (*Suppl 4*), 40–46.
4. Beck, A.E., McMillin, M.J., Gildersleeve, H.I.S., Kezele, P.R., Shively, K.M., Carey, J.C., Regnier, M., and Bamshad, M.J. (2013). Spectrum of mutations that cause distal arthrogryposis types 1 and 2B. Am. J. Med. Genet. A. *161A*, 550–555.
5. McMillin, M.J., Below, J.E., Shively, K.M., Beck, A.E., Gildersleeve, H.I., Pinner, J., Gogola, G.R., Hecht, J.T., Grange, D.K., Harris, D.J., et al.; University of Washington Center for Mendelian Genomics (2013). Mutations in ECEL1 cause distal arthrogryposis type 5D. Am. J. Hum. Genet. *92*, 150–156.
6. Hirata, H., Nanda, I., van Riesen, A., McMichael, G., Hu, H., Hambrock, M., Papon, M.-A., Fischer, U., Marouillat, S., Ding, C., et al. (2013). ZC4H2 mutations are associated with arthrogryposis multiplex congenita and intellectual disability through impairment of central and peripheral synaptic plasticity. Am. J. Hum. Genet. *92*, 681–695.
7. Laquérriere, A., Maluenda, J., Camus, A., Fontenas, L., Dieterich, K., Nolent, F., Zhou, J., Monnier, N., Latour, P., Gentil, D., et al. (2014). Mutations in CNTNAP1 and ADCY6 are responsible for severe arthrogryposis multiplex congenita with axoglial defects. Hum. Mol. Genet. *23*, 2279–2289.
8. Abicht, A., Müller, J., and Lochmüller, H. (2012). Congenital Myasthenic Syndromes. In Congenital Myasthenic Syndromes, R.A. Pagon, M.P. Adam, H.H. Ardinger, S.E. Wallace, A. Amemiya, L.J. Bean, T.D. Bird, C.R. Dolan, C.-T. Fong, and R.J. Smith, et al., eds. (Seattle, WA: University of Washington, Seattle).
9. Vogt, J., Harrison, B.J., Spearman, H., Cossins, J., Vermeer, S., ten Cate, L.N., Morgan, N.V., Beeson, D., and Maher, E.R. (2008). Mutation analysis of CHRNA1, CHRNB1, CHRND, and RAPSN genes in multiple pterygium syndrome/fetal akinesia patients. Am. J. Hum. Genet. *82*, 222–227.
10. Cullinane, A.R., Straatman-Iwanowska, A., Zaucker, A., Wakabayashi, Y., Bruce, C.K., Luo, G., Rahman, F., Gürakan, F., Utine, E., Özkan, T.B., et al. (2010). Mutations in VIPAR cause an arthrogryposis, renal dysfunction and cholestasis syndrome phenotype with defects in epithelial polarization. Nat. Genet. *42*, 303–312.

11. Morgan, J.A., and Marcus, P.S. (2010). Prenatal diagnosis and management of intrauterine fracture. Obstet. Gynecol. Surv. *65*, 249–259.
12. Hall, J.G., Aldinger, K.A., and Tanaka, K.I. (2014). Amyoplasia revisited. Am. J. Med. Genet. A. *164A*, 700–730.
13. Greenberg, F., Fenolio, K.R., Hejtmancik, J.F., Armstrong, D., Willis, J.K., Shapira, E., Huntington, H.W., and Haun, R.L. (1988). X-linked infantile spinal muscular atrophy. Am. J. Dis. Child. *142*, 217–219.
14. Ramser, J., Ahearn, M.E., Lenski, C., Yariz, K.O., Hellebrand, H., von Rhein, M., Clark, R.D., Schmutzler, R.K., Lichtner, P., Hoffman, E.P., et al. (2008). Rare missense and synonymous variants in UBE1 are associated with X-linked infantile spinal muscular atrophy. Am. J. Hum. Genet. *82*, 188–193.
15. Shaheen, R., Al-Owain, M., Sakati, N., Alzayed, Z.S., and Alkuraya, F.S. (2010). FKBP10 and Bruck syndrome: phenotypic heterogeneity or call for reclassification? Am. J. Hum. Genet. *87*, 306–307, author reply 308.
16. Narkis, G., Ofir, R., Landau, D., Manor, E., Volokita, M., Hershkowitz, R., Elbedour, K., and Birk, O.S. (2007). Lethal contractural syndrome type 3 (LCCS3) is caused by a mutation in PIP5K1C, which encodes PIPKI γ of the phophatidylinsitol pathway. Am. J. Hum. Genet. *81*, 530–539.
17. Ryan, M.M., Schnell, C., Strickland, C.D., Shield, L.K., Morgan, G., Iannaccone, S.T., Laing, N.G., Beggs, A.H., and North, K.N. (2001). Nemaline myopathy: a clinical study of 143 cases. Ann. Neurol. *50*, 312–320.
18. Garcia-Angarita, N., Kirschner, J., Heiliger, M., Thirion, C., Walter, M.C., Schnittfeld-Acarlioglu, S., Albrecht, M., Müller, K., Wieczorek, D., Lochmüller, H., and Krause, S. (2009). Severe nemaline myopathy associated with consecutive mutations E74D and H75Y on a single ACTA1 allele. Neuromuscul. Disord. *19*, 481–484.
19. Ravenscroft, G., Miyatake, S., Lehtokari, V.-L., Todd, E.J., Vornanen, P., Yau, K.S., Hayashi, Y.K., Miyake, N., Tsurusaki, Y., Doi, H., et al. (2013). Mutations in KLHL40 are a frequent cause of severe autosomal-recessive nemaline myopathy. Am. J. Hum. Genet. *93*, 6–18.
20. García-Cabezas, M.A., García-Alix, A., Martín, Y., Gutiérrez, M., Hernández, C., Rodríguez, J.I., and Morales, C. (2004). Neonatal spinal muscular atrophy with multiple contractures, bone fractures, respiratory insufficiency and 5q13 deletion. Acta Neuropathol. *107*, 475–478.
21. Kelly, T.E., Amoroso, K., Ferre, M., Blanco, J., Allinson, P., and Prior, T.W. (1999). Spinal muscular atrophy variant with congenital fractures. Am. J. Med. Genet. *87*, 65–68.
22. Courtens, W., Johansson, A.-B., Dachy, B., Avni, F., Telerman-Toppet, N., and Scheffer, H. (2002). Infantile spinal muscular atrophy variant with congenital fractures in a female neonate: evidence for autosomal recessive inheritance. J. Med. Genet. *39*, 74–77.
23. Van Toorn, R., Davies, J., and Wilmshurst, J.M. (2002). Spinal muscular atrophy with congenital fractures: postmortem analysis. J. Child Neurol. *17*, 721–723.
24. Felderhoff-Mueser, U., Grohmann, K., Harder, A., Stadelmann, C., Zerres, K., Bührer, C., and Obladen, M. (2002). Severe spinal muscular atrophy variant associated with congenital bone fractures. J. Child Neurol. *17*, 718–721.
25. Spiegelman, B.M., and Heinrich, R. (2004). Biological control through regulated transcriptional coactivators. Cell *119*, 157–167.
26. Mouchiroud, L., Eichner, L.J., Shaw, R.J., and Auwerx, J. (2014). Transcriptional coregulators: fine-tuning metabolism. Cell Metab. *20*, 26–40.
27. Hahm, J.B., and Privalsky, M.L. (2013). Research resource: identification of novel coregulators specific for thyroid hormone receptor-β2. Mol. Endocrinol. *27*, 840–859.
28. Auboeuf, D., Dowhan, D.H., Kang, Y.K., Larkin, K., Lee, J.W., Berget, S.M., and O'Malley, B.W. (2004). Differential recruitment of nuclear receptor coactivators may determine alternative RNA splice site choice in target genes. Proc. Natl. Acad. Sci. USA *101*, 2270–2274.
29. Jung, D.-J., Sung, H.-S., Goo, Y.-W., Lee, H.M., Park, O.K., Jung, S.-Y., Lim, J., Kim, H.-J., Lee, S.-K., Kim, T.S., et al. (2002). Novel transcription coactivator complex containing activating signal cointegrator 1. Mol. Cell. Biol. *22*, 5203–5211.
30. Iyer, L.M., Burroughs, A.M., and Aravind, L. (2006). The ASCH superfamily: novel domains with a fold related to the PUA domain and a potential role in RNA metabolism. Bioinformatics *22*, 257–263.
31. Mazumder, R., Iyer, L.M., Vasudevan, S., and Aravind, L. (2002). Detection of novel members, structure-function analysis and evolutionary classification of the 2H phosphoesterase superfamily. Nucleic Acids Res. *30*, 5229–5243.
32. Seelow, D., and Schuelke, M. (2012). HomozygosityMapper2012–bridging the gap between homozygosity mapping and deep sequencing. Nucleic Acids Res. *40*, W516–W520.
33. von Renesse, A., Petkova, M.V., Lützkendorf, S., Heinemeyer, J., Gill, E., Hübner, C., von Moers, A., Stenzel, W., and Schuelke, M. (2014). POMK mutation in a family with congenital muscular dystrophy with merosin deficiency, hypomyelination, mild hearing deficit and intellectual disability. J. Med. Genet. *51*, 275–282.
34. Li, H. (2013). Aligning sequence reads, clone sequences and assembly contigs with BWA-MEM. arXiv, arXiv:1303.3997, http://arxiv.org/pdf/1303.3997.pdf.
35. McKenna, A., Hanna, M., Banks, E., Sivachenko, A., Cibulskis, K., Kernytsky, A., Garimella, K., Altshuler, D., Gabriel, S., Daly, M., and DePristo, M.A. (2010). The Genome Analysis Toolkit: a MapReduce framework for analyzing next-generation DNA sequencing data. Genome Res. *20*, 1297–1303.
36. Schwarz, J.M., Rödelsperger, C., Schuelke, M., and Seelow, D. (2010). MutationTaster evaluates disease-causing potential of sequence alterations. Nat. Methods *7*, 575–576.
37. Trapnell, C., Roberts, A., Goff, L., Pertea, G., Kim, D., Kelley, D.R., Pimentel, H., Salzberg, S.L., Rinn, J.L., and Pachter, L. (2012). Differential gene and transcript expression analysis of RNA-seq experiments with TopHat and Cufflinks. Nat. Protoc. *7*, 562–578.
38. Schuelke, M., and Cervós-Navarro, J. (1998). Degenerative changes in unmyelinated nerve fibers in late-infantile neuronal ceroidlipofuscinosis. A morphometric study of conjunctival biopsy specimens. Acta Neuropathol. *95*, 175–183.
39. Rajab, A., Straub, V., McCann, L.J., Seelow, D., Varon, R., Barresi, R., Schulze, A., Lucke, B., Lützkendorf, S., Karbasiyan, M., et al. (2010). Fatal cardiac arrhythmia and long-QT syndrome in a new form of congenital generalized lipodystrophy with muscle rippling (CGL4) due to PTRF-CAVIN mutations. PLoS Genet. *6*, e1000874.
40. Wirtz, S., and Schuelke, M. (2011). Region-specific expression of mitochondrial complex I genes during murine brain development. PLoS ONE *6*, e18897.

41. Naganawa, Y., and Hirata, H. (2011). Developmental transition of touch response from slow muscle-mediated coilings to fast muscle-mediated burst swimming in zebrafish. Dev. Biol. *355*, 194–204.
42. Kuehn, H., Liberzon, A., Reich, M., and Mesirov, J.P. (2008). Using GenePattern for Gene Expression Analysis. In Current Protocols in Bioinformatics (John Wiley & Sons) http://dx.doi.org/10.1002/0471250953, bi0712s22.
43. Ashburner, M., Ball, C.A., Blake, J.A., Botstein, D., Butler, H., Cherry, J.M., Davis, A.P., Dolinski, K., Dwight, S.S., Eppig, J.T., et al.; The Gene Ontology Consortium (2000). Gene ontology: tool for the unification of biology. Nat. Genet. *25*, 25–29.
44. Reiner, A., Yekutieli, D., and Benjamini, Y. (2003). Identifying differentially expressed genes using false discovery rate controlling procedures. Bioinformatics *19*, 368–375.
45. Robinson, P.N., Köhler, S., Bauer, S., Seelow, D., Horn, D., and Mundlos, S. (2008). The Human Phenotype Ontology: a tool for annotating and analyzing human hereditary disease. Am. J. Hum. Genet. *83*, 610–615.
46. Origuchi, Y. (1981). Quantitative histological study in the sural nerves of children. Brain Dev. *3*, 395–402.
47. Schröder, J.M., Bohl, J., and Brodda, K. (1978). Changes of the ratio between myelin thickness and axon diameter in the human developing sural nerve. Acta Neuropathol. *43*, 169–178.
48. Shield, L.K., King, R.H.M., and Thomas, P.K. (1986). A morphometric study of human fetal sural nerve. Acta Neuropathol. *70*, 60–70.
49. Halliday, K.E., Broderick, N.J., Somers, J.M., and Hawkes, R. (2011). Dating fractures in infants. Clin. Radiol. *66*, 1049–1054.
50. Sossi, V., Giuli, A., Vitali, T., Tiziano, F., Mirabella, M., Antonelli, A., Neri, G., and Brahe, C. (2001). Premature termination mutations in exon 3 of the SMN1 gene are associated with exon skipping and a relatively mild SMA phenotype. Eur. J. Hum. Genet. *9*, 113–120.
51. Colombo, E.A., Fontana, L., Roversi, G., Negri, G., Castiglia, D., Paradisi, M., Zambruno, G., and Larizza, L. (2014). Novel physiological RECQL4 alternative transcript disclosed by molecular characterisation of Rothmund-Thomson Syndrome sibs with mild phenotype. Eur. J. Hum. Genet. *22*, 1298–1304.
52. Schmid, F., Glaus, E., Cremers, F.P.M., Kloeckener-Gruissem, B., Berger, W., and Neidhardt, J. (2010). Mutation- and tissue-specific alterations of RPGR transcripts. Invest. Ophthalmol. Vis. Sci. *51*, 1628–1635.
53. Demir, E., Sabatelli, P., Allamand, V., Ferreiro, A., Moghadaszadeh, B., Makrelouf, M., Topaloglu, H., Echenne, B., Merlini, L., and Guicheney, P. (2002). Mutations in COL6A3 cause severe and mild phenotypes of Ullrich congenital muscular dystrophy. Am. J. Hum. Genet. *70*, 1446–1458.
54. Ruzzi, L., Pas, H., Posteraro, P., Mazzanti, C., Didona, B., Owaribe, K., Meneguzzi, G., Zambruno, G., Castiglia, D., and D'Alessio, M. (2001). A homozygous nonsense mutation in type XVII collagen gene (COL17A1) uncovers an alternatively spliced mRNA accounting for an unusually mild form of non-Herlitz junctional epidermolysis bullosa. J. Invest. Dermatol. *116*, 182–187.
55. Kim, H.-J., Yi, J.-Y., Sung, H.-S., Moore, D.D., Jhun, B.H., Lee, Y.C., and Lee, J.W. (1999). Activating signal cointegrator 1, a novel transcription coactivator of nuclear receptors, and its cytosolic localization under conditions of serum deprivation. Mol. Cell. Biol. *19*, 6323–6332.
56. Ma, L., Yu, Y.-M., Guo, Y., Hart, R.P., and Schachner, M. (2012). Cysteine- and glycine-rich protein 1a is involved in spinal cord regeneration in adult zebrafish. Eur. J. Neurosci. *35*, 353–365.
57. van der Knaap, M.S., Leegwater, P.A.J., Könst, A.A.M., Visser, A., Naidu, S., Oudejans, C.B.M., Schutgens, R.B.H., and Pronk, J.C. (2002). Mutations in each of the five subunits of translation initiation factor eIF2B can cause leukoencephalopathy with vanishing white matter. Ann. Neurol. *51*, 264–270.
58. Lee, J.W., Choi, H.S., Gyuris, J., Brent, R., and Moore, D.D. (1995). Two classes of proteins dependent on either the presence or absence of thyroid hormone for interaction with the thyroid hormone receptor. Mol. Endocrinol. *9*, 243–254.
59. Li, S., Czubryt, M.P., McAnally, J., Bassel-Duby, R., Richardson, J.A., Wiebel, F.F., Nordheim, A., and Olson, E.N. (2005). Requirement for serum response factor for skeletal muscle growth and maturation revealed by tissue-specific gene deletion in mice. Proc. Natl. Acad. Sci. USA *102*, 1082–1087.
60. Wickramasinghe, S.R., Alvania, R.S., Ramanan, N., Wood, J.N., Mandai, K., and Ginty, D.D. (2008). Serum response factor mediates NGF-dependent target innervation by embryonic DRG sensory neurons. Neuron *58*, 532–545.
61. Stern, S., Haverkamp, S., Sinske, D., Tedeschi, A., Naumann, U., Di Giovanni, S., Kochanek, S., Nordheim, A., and Knöll, B. (2013). The transcription factor serum response factor stimulates axon regeneration through cytoplasmic localization and cofilin interaction. J. Neurosci. *33*, 18836–18848.
62. Chen, J., Yuan, K., Mao, X., Miano, J.M., Wu, H., and Chen, Y. (2012). Serum response factor regulates bone formation via IGF-1 and Runx2 signals. J. Bone Miner. Res. *27*, 1659–1668.
63. Wang, X., Lee, G., Liebhaber, S.A., and Cooke, N.E. (1992). Human cysteine-rich protein. A member of the LIM/double-finger family displaying coordinate serum induction with c-myc. J. Biol. Chem. *267*, 9176–9184.
64. Chang, D.F., Belaguli, N.S., Iyer, D., Roberts, W.B., Wu, S.-P., Dong, X.-R., Marx, J.G., Moore, M.S., Beckerle, M.C., Majesky, M.W., and Schwartz, R.J. (2003). Cysteine-rich LIM-only proteins CRP1 and CRP2 are potent smooth muscle differentiation cofactors. Dev. Cell *4*, 107–118.
65. Visel, A., Thaller, C., and Eichele, G. (2004). GenePaint.org: an atlas of gene expression patterns in the mouse embryo. Nucleic Acids Res. *32*, D552–D556.
66. Miyasaka, K.Y., Kida, Y.S., Sato, T., Minami, M., and Ogura, T. (2007). Csrp1 regulates dynamic cell movements of the mesendoderm and cardiac mesoderm through interactions with Dishevelled and Diversin. Proc. Natl. Acad. Sci. USA *104*, 11274–11279.
67. Oldham, M.C., Konopka, G., Iwamoto, K., Langfelder, P., Kato, T., Horvath, S., and Geschwind, D.H. (2008). Functional organization of the transcriptome in human brain. Nat. Neurosci. *11*, 1271–1282.
68. Visser, W.E., Swagemakers, S.M.A., Őzgűr, Z., Schot, R., Verheijen, F.W., van Ijcken, W.F.J., van der Spek, P.J., and Visser, T.J. (2010). Transcriptional profiling of fibroblasts from patients with mutations in MCT8 and comparative analysis with the human brain transcriptome. Hum. Mol. Genet. *19*, 4189–4200.
69. Roet, K.C.D., Franssen, E.H.P., de Bree, F.M., Essing, A.H.W., Zijlstra, S.-J.J., Fagoe, N.D., Eggink, H.M., Eggers, R., Smit, A.B., van Kesteren, R.E., and Verhaagen, J. (2013). A multilevel screening strategy defines a molecular fingerprint of proregenerative olfactory ensheathing cells and identifies SCARB2,

a protein that improves regenerative sprouting of injured sensory spinal axons. J. Neurosci. *33*, 11116–11135.

70. Unterlauft, J.D., Eichler, W., Kuhne, K., Yang, X.M., Yafai, Y., Wiedemann, P., Reichenbach, A., and Claudepierre, T. (2012). Pigment epithelium-derived factor released by Müller glial cells exerts neuroprotective effects on retinal ganglion cells. Neurochem. Res. *37*, 1524–1533.
71. Bilak, M.M.P., Corse, A.M., Bilak, S.R.P., Lehar, M., Tombran-Tink, J., and Kuncl, R.W.M. (1999). Pigment epithelium-derived factor (PEDF) protects motor neurons from chronic glutamate-mediated neurodegeneration. J. Neuropathol. Exp. Neurol. *58*, 719–728.
72. Carulli, D., Pizzorusso, T., Kwok, J.C.F., Putignano, E., Poli, A., Forostyak, S., Andrews, M.R., Deepa, S.S., Glant, T.T., and Fawcett, J.W. (2010). Animals lacking link protein have attenuated perineuronal nets and persistent plasticity. Brain *133*, 2331–2347.
73. Wise, G.E., Yao, S., Zhang, Q., and Ren, Y. (2002). Inhibition of osteoclastogenesis by the secretion of osteoprotegerin in vitro by rat dental follicle cells and its implications for tooth eruption. Arch. Oral Biol. *47*, 247–254.
74. Roudier, M.P., Bain, S.D., and Dougall, W.C. (2006). Effects of the RANKL inhibitor, osteoprotegerin, on the pain and histopathology of bone cancer in rats. Clin. Exp. Metastasis *23*, 167–175.
75. Simonet, W.S., Lacey, D.L., Dunstan, C.R., Kelley, M., Chang, M.-S., Lüthy, R., Nguyen, H.Q., Wooden, S., Bennett, L., Boone, T., et al. (1997). Osteoprotegerin: a novel secreted protein involved in the regulation of bone density. Cell *89*, 309–319.

The American Journal of Human Genetics, Volume *98*

Supplemental Information

Mutations in Subunits of the Activating Signal Cointegrator 1 Complex Are Associated with Prenatal Spinal Muscular Atrophy and Congenital Bone Fractures

Ellen Knierim, Hiromi Hirata, Nicole I. Wolf, Susanne Morales-Gonzalez, Gudrun Schottmann, Yu Tanaka, Sabine Rudnik-Schöneborn, Mickael Orgeur, Klaus Zerres, Stefanie Vogt, Anne van Riesen, Esther Gill, Franziska Seifert, Angelika Zwirner, Janbernd Kirschner, Hans Hilmar Goebel, Christoph Hübner, Sigmar Stricker, David Meierhofer, Werner Stenzel, and Markus Schuelke

Table of contents

Supplemental figures

Morphometric analysis of the sural nerve

Figure S1 Representative cross sections of sural nerve biopsy specimens

Figure S2 Morphometric analysis of myelinated axon diameters of sural nerve biopsies

Results of the autozygosity mapping in three families

Figure S3 Autozygosity mapping of Family A

Figure S4 Autozygosity mapping of Family B

Figure S5 Autozygosity mapping of Family D

In-situ hybridization of whole E17.5 mouse embryos

Figure S6 Comparison of in-situ intensities for *Trip4* antisense and sense probes

Figure S7 Comparison of in-situ intensities for *Ascc1* antisense and sense probes

Quantification of morpholino injection into zebrafish

Figure S8 Morpholino mediated exon skipping in *ascc1* and *trip4* transcripts

Figure S9 Morpholino mediated knockdown of *ascc1* and *trip4*

Figure S10 Use of alternative MO2 constructs for *trip4* and *ascc1* knockdown

Figure S11 Rescue of MO-knockdown with wildtype and mutant mRNAs

Expression of SRF responsive genes after serum challenge

Figure S12 Expression of known SRF responsive target genes after serum challenge

Subcellular location of the ASC-1 complex and of the CSRP1 protein

Figure S13 Subcellular localization of the ASC-1 complex and of the CSRP1 protein after serum starvation and challenge

Multiple species alignment of TRIP4 and ASCC1 amino acid sequences

Figure S14 Multiple species alignment of *TRIP4*

Figure S15 Multiple species alignment of *ASCC1*

Co-immunoprecipitation with antibodies against three subunits of the ASC-1 complex

Figure S16 Immunoprecipitation with an anti-TRIP4 antibody

Figure S17 Immunoprecipitation with an anti-ASCC1 antibody

Figure S18 Immunoprecipitation with an anti-ASCC2 antibody

HCD spectra of peptides from interacting proteins

Figure S19 MS spectra of two identified TRIP4 peptides

Figure S20 MS spectra of two identified ASCC1 peptides

Figure S21 MS spectra of two identified ASCC2 peptides

Figure S22 MS spectra of two identified ASCC3 peptides

Figure S23 MS spectrum of one identified CSRP1 peptide

Supplemental tables

Morphometric analysis of the sural nerve
Table S1 Fiber density of myelinated fibers in patients and control

Coverage details of the exome sequencing
Table S2 Coverage details of three WES datasets

Quantification of morpholino injection into zebrafish
Table S3 Quantification of the "coiling" behavior of morphants and controls
Table S4 Quantification of the "coiling" behavior using an alternative morpholino
Table S5 Quantification of the density of neuromuscular junctions

Quantification of gene expression in patient and control fibroblasts
Table S6 Differentially regulated genes in *ASCC1* mutant versus control skin fibroblasts

Mass spectrometric analysis of peptides from immunoprecipitations
Table S7 Mass spectrometric analysis of peptides from immunoprecipitations

Oligonucleotides for sequencing, cloning, in vitro mutagenesis and morpholino mediated knockdown
Table S8 Oligonucleotides used for molecular genetics experiments

Antibodies for immunostaining, immunoprecipitation, and Western blot
Table S9 List of used antibodies

Morphometric analysis of the sural nerve

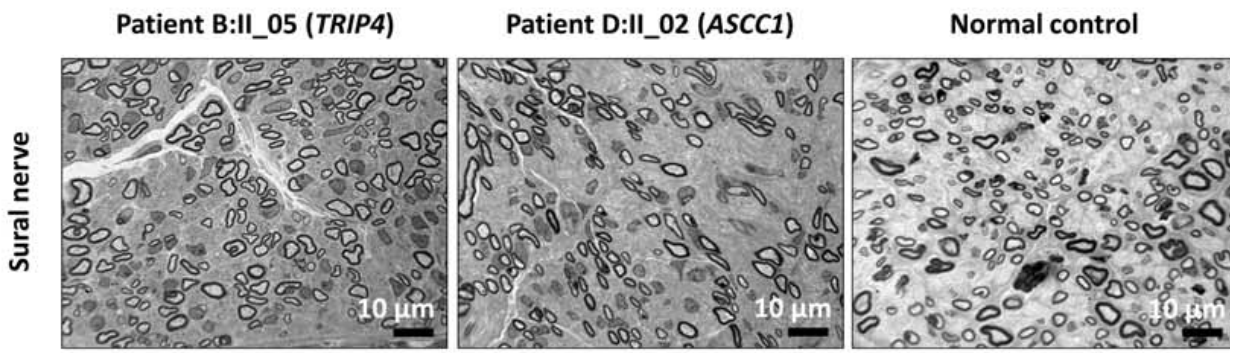

Figure S1. **Representative cross sections of sural nerve biopsy specimens** Five of such visual fields were analyzed for each nerve in two patients and one age-matched control.

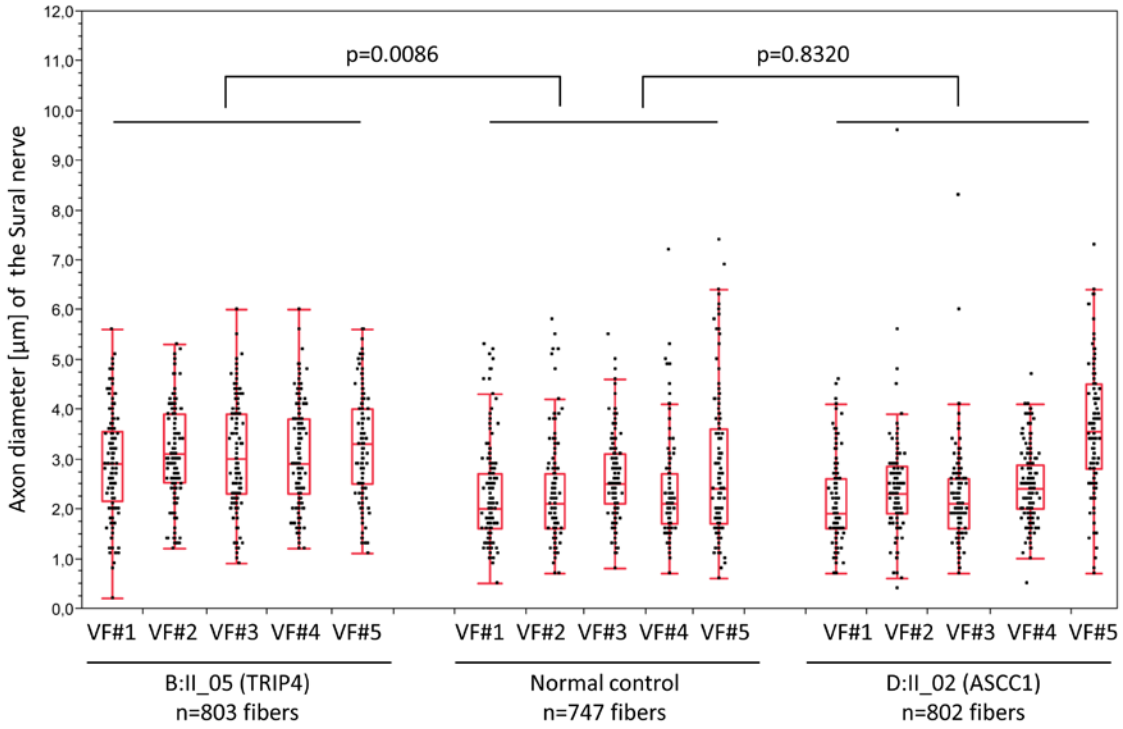

Figure S2. **Morphometric analysis of myelinated axon diameters of sural nerve biopsies.** Sural nerve biopsies were fixed in glutaraldehyde, embedded in Epon®. Semithin sections were stained with methylene blue or with paraphenylene diamine to visualize the myelin sheaths. From each nerve five full visual fields that were entirely filled with myelinated axons were photographed, together with an object micrometer scale using a 100x objective on a Leica DML3000 inverted microscope. The images were recorded in bright field with a cooled SPOT RT3 CCD-camera (1,600 x 1,200 px). Axon diameters were measured morphometrically using the free ImageJ v1.37a program. The axon diameters were depicted in a multiple dot/box blot. The boxes depict the median, 10^{th}, 25^{th}, 75^{th}, and 90^{th} percentiles; p-values were calculated with the non-parametric Man-Whitney U-test.

Results of the autozygosity mapping in three families

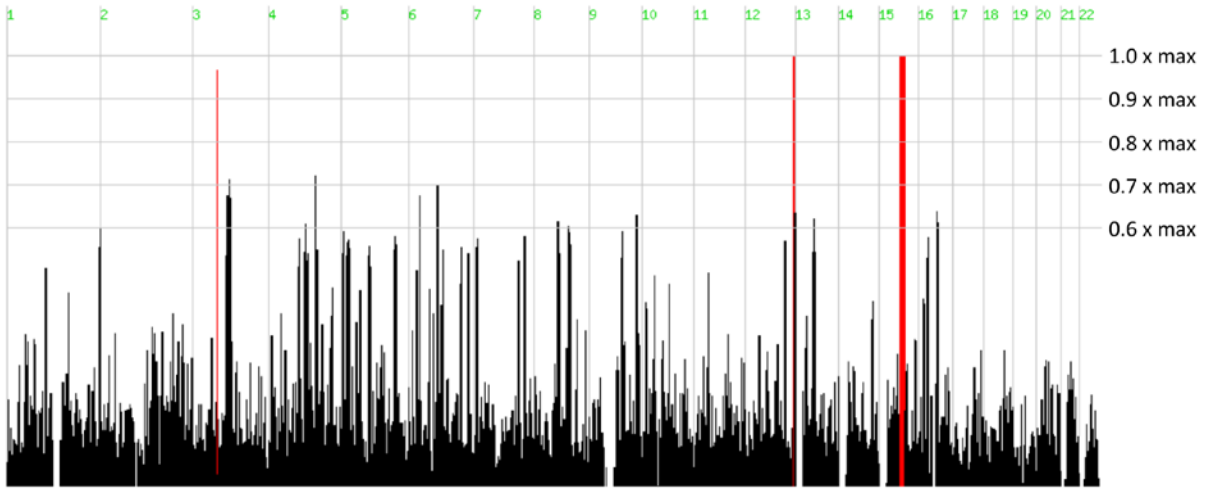

Figure S3. **Autozygosity mapping of Family A** Two affected individuals were used for the analysis. The red bars depict the autozygous regions at: Chr03:64,230,433-65,658,852 (rs3911778-rs6803573), Chr12:129,242,824-132,057,829 (rs7966499-rs7963314), and Chr15:53,697,249-66,260,894 (rs1021746-rs333556).

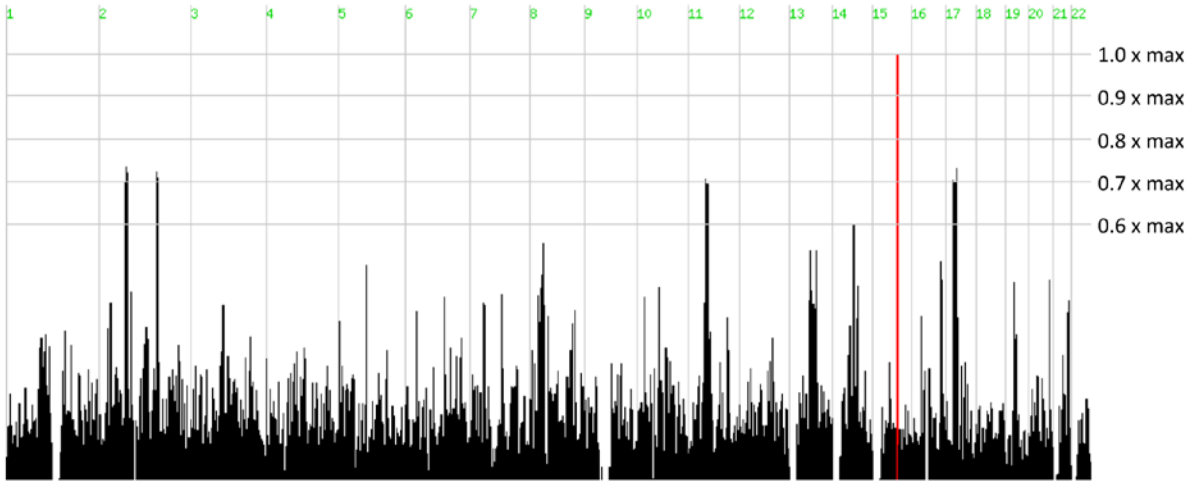

Figure S4. **Autozygosity mapping of Family B** Three affected and two unaffected individuals were used for the analysis. The red bars depict the regions that were only homozygous in the patients and not in the unaffected family members at Chr15:63,594,231-68 726 159 (rs12910654-rs12915814). A *shared autozygous region* between Families A and B comprised an interval on Chr15:63,594,231-66,260,894 (rs12910654-rs333556) that contained 38 protein-coding genes.

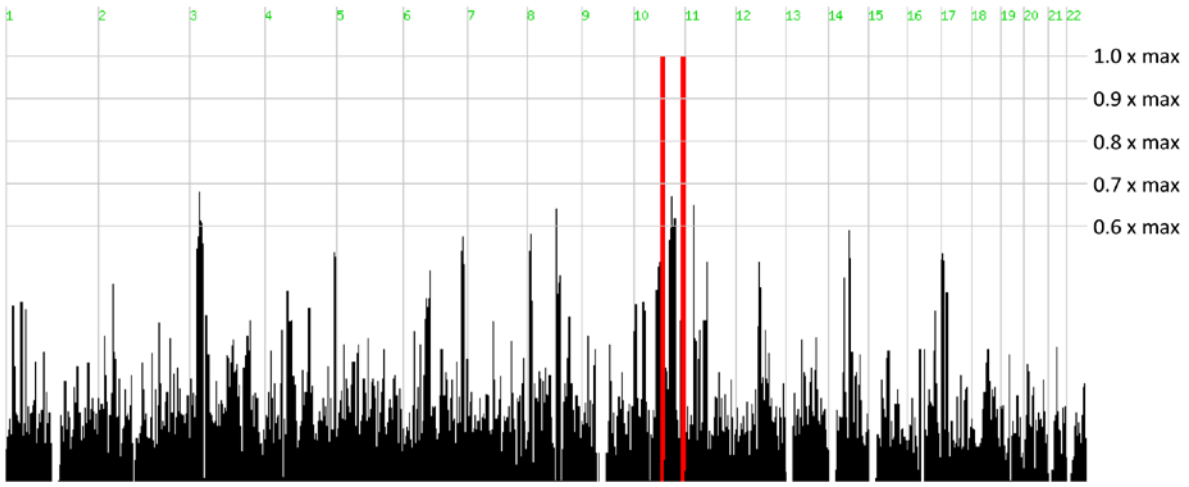

Figure S5. **Autozygosity mapping of Family D** Two affected and one unaffected individual were used for the analysis. The red bars depict the regions that were only homozygous in the patients and not in the unaffected family member at Chr10:71,613,489-81,169,345 (rs2683563-rs10824752) and Chr10:124,114,432-135,422,505 (rs7905027-rs4498943) comprising 196 protein coding genes.

In-situ hybridization of whole E17.5 mouse embryos

Figure S6. **Comparison of in-situ intensities for *Trip4* antisense and sense probes.** In-situ hybridization of a parasagittal section of an E17.5 C57BL6/J embryo with a *Trip4* antisense probe (left) and the corresponding sense probe (right). Both DIG-labeled RNA-probes were generated from the same plasmid via transcription from the T3 promoter (antisense) or the T7 promoter (sense) of the pCR-Script plasmid. Due to the large size of the embryo single sub-images are stitched together to represent the entire embryo on a single image. Both images have been recorded with the identical illumination settings.

Figure S7. **Comparison of in-situ intensities for *Ascc1* antisense and sense probes.** In-situ hybridization of a parasagittal section of an E17.5 C57BL6/J embryo with an *Ascc1* antisense probe (left) and the corresponding sense probe (right). Both DIG-labeled RNA-probes were generated from the same plasmid *via* transcription from the T3 promoter (antisense) or the T7 promoter (sense) of the pCR-Script plasmid. Due to the large size of the embryo single sub-images are stitched together to represent the entire embryo on a single image. Both images have been recorded with the identical illumination settings.

Quantification of morpholino injection into zebrafish

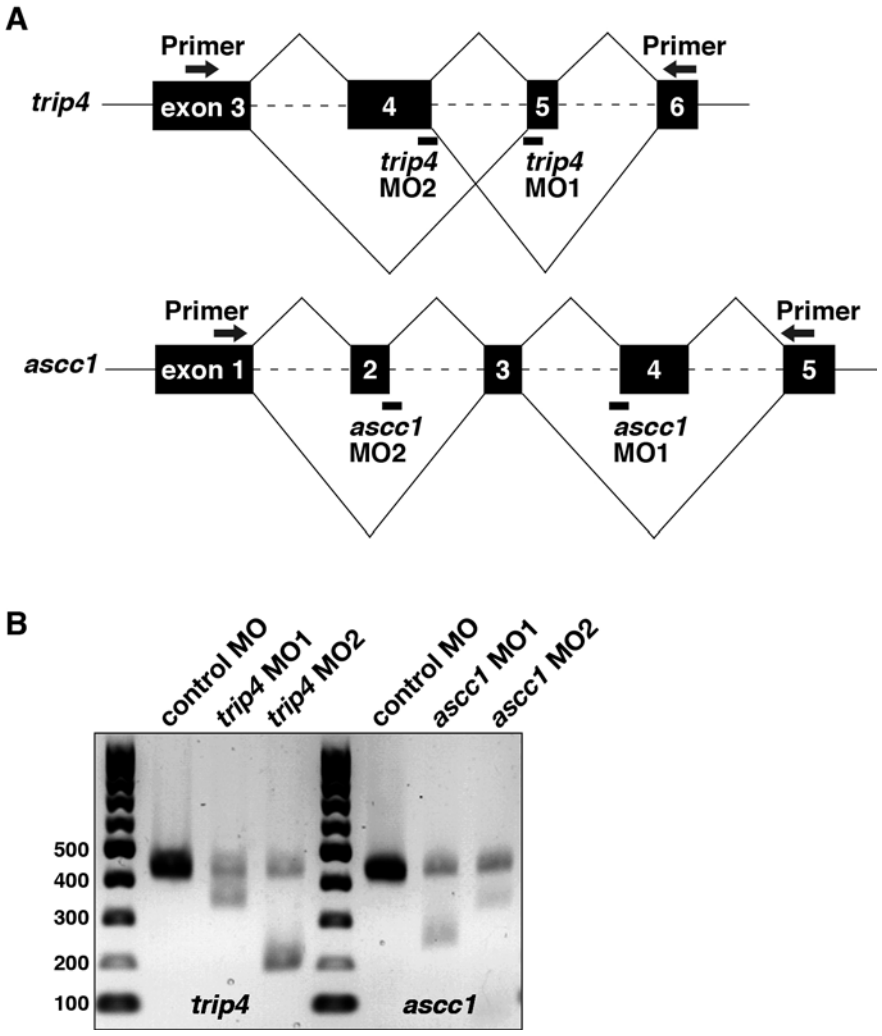

Figure S8. **Morpholino mediated exon skipping in *ascc1* and *trip4* transcripts. (A)** Location of the MOs at the *trip4* and *ascc1* splice junctions, position of the oligonucleotide primers used for RT-PCR and exon skipping patterns. **(B)** Agarose gel electrophoresis of *trip4* and *ascc1* RT-PCR products in differently injected zebrafish embryos verifying exon skipping. The sizes of the skipped exons are: *trip4* MO1 = exon 5 (79 bp); *trip4* MO2 = exon 4 (219 bp); *ascc1* MO1 = exon 4 (180 bp); *ascc1* MO2 = exon 2 (100 bp). red = in-frame deletion, blue = out-of-frame deletion

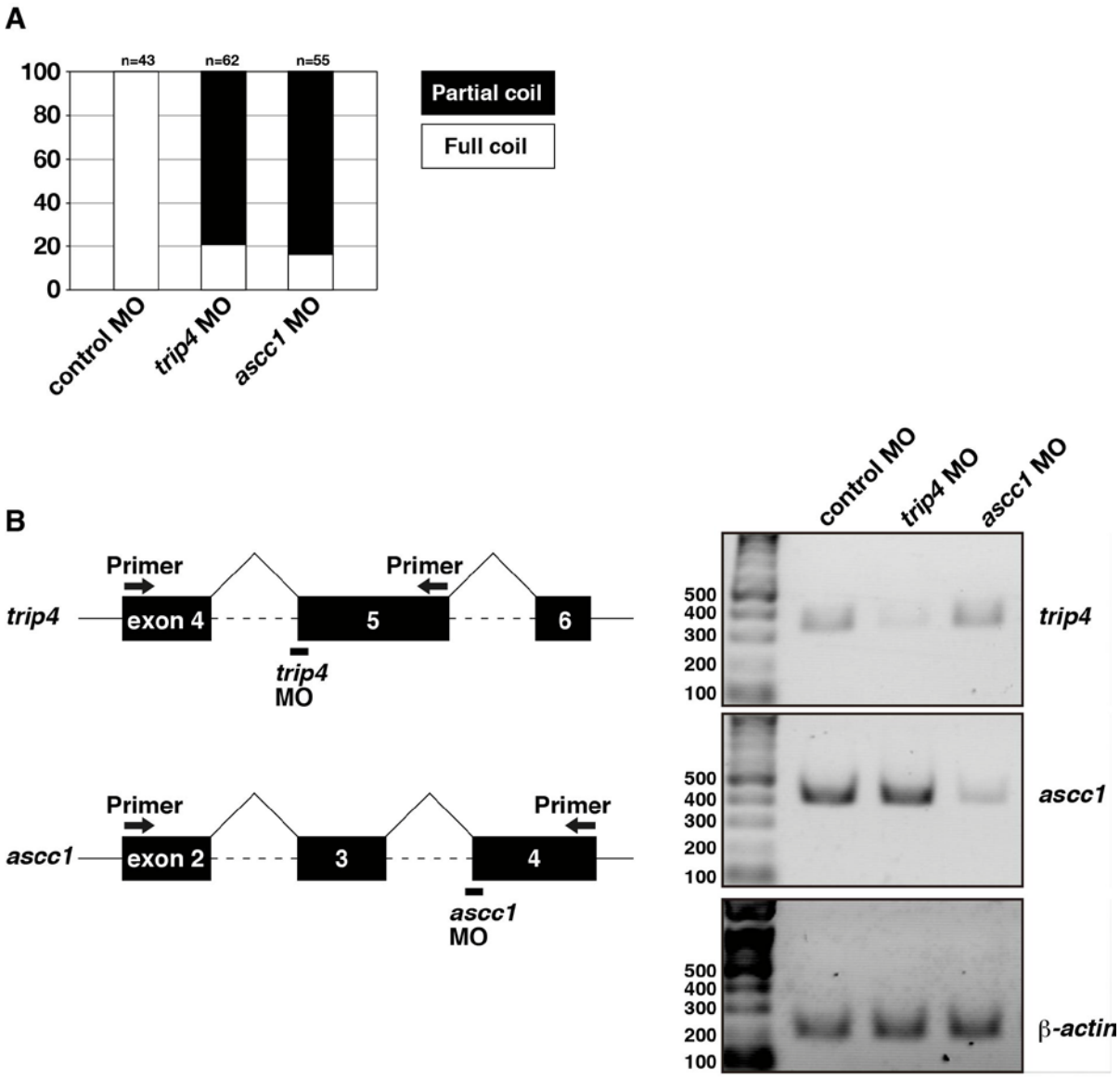

Figure S9. **Morpholino mediated knockdown of *ascc1* and *trip4*. (A)** Effect of control, *trip4* and *ascc1* MO (5 ng each) mediated knockdown on the ability of the 30 hpf zebrafish embryos for "full coil" or "partial coil". **(B)** ***Left panel:*** Location of the MOs at *trip4* and *ascc1* splice junctions and position of the oligonucleotide primers used for RT-PCR. ***Right panels:*** Agarose gel electrophoresis of *trip4* and *ascc1* RT-PCR products in differently injected zebrafish embryos verifying the specific knockdown of the intended targets. β-actin mRNA was taken as reference.

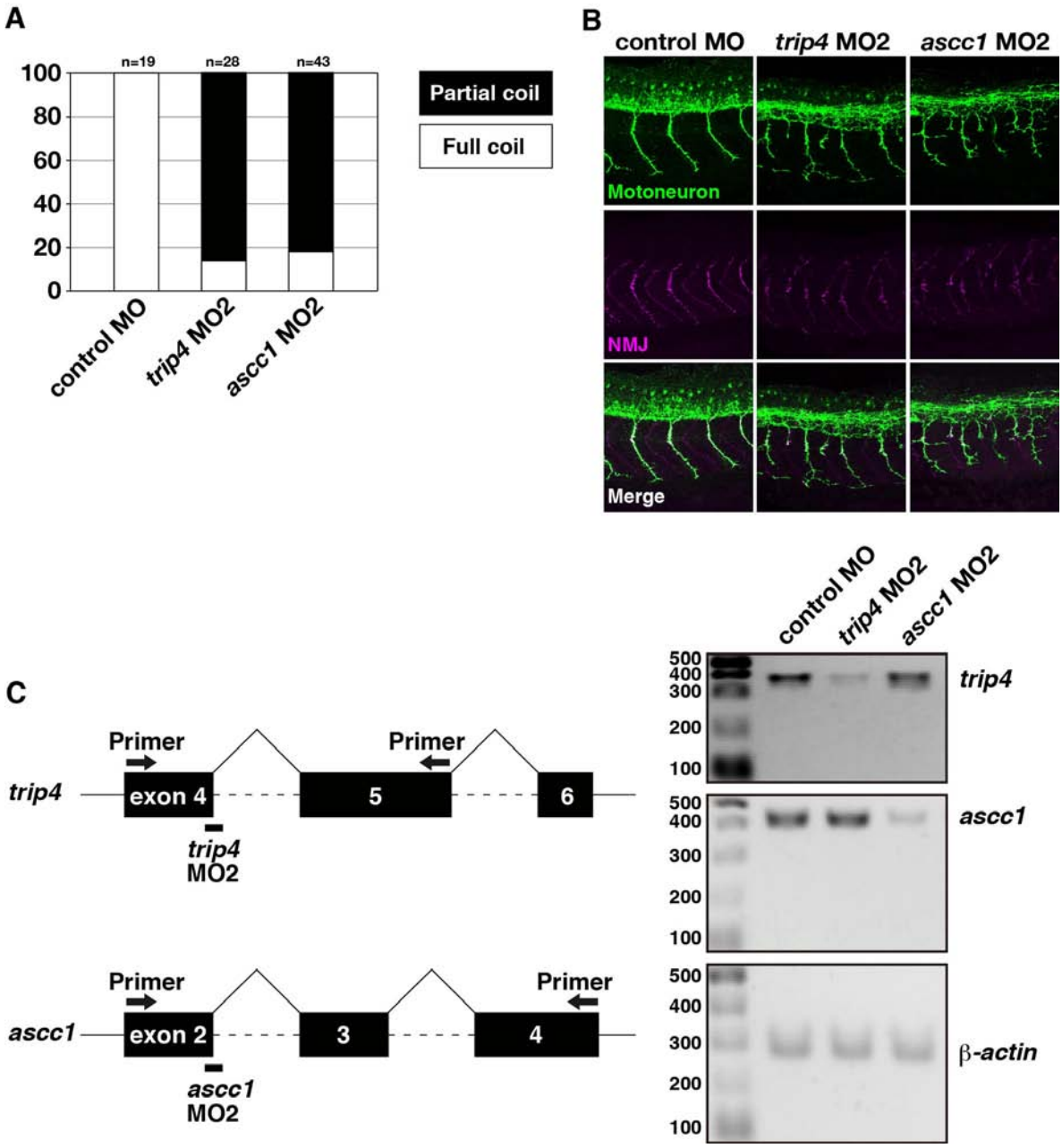

Figure S10. **Use of alternative MO2 constructs for *trip4* and *ascc1* knockdown. (A)** Effect of control, *trip4* and *ascc1* MO2 (5 ng each) mediated knockdown on the ability of the 30 hpf zebrafish embryos for "full coil" or "partial coil". **(B)** The alternative *trip4* and *ascc1* MO2s have the same specificity to generate the morphologic abnormalities of the α-motoneuron and the neuromuscular junction as the respective MOs (see Figure 3C for comparison), hence verifying the specificity of the effect. **(C)** ***Left panel:*** Location of the MO2s at *trip4* and *ascc1* splice junctions and position of the oligonucleotide primers used for RT-PCR. ***Right panels:*** Agarose gel electrophoresis of *trip4* and *ascc1* RT-PCR products in differently injected zebrafish embryos verifying the specific knockdown of the intended targets. β-actin mRNA was taken as reference.

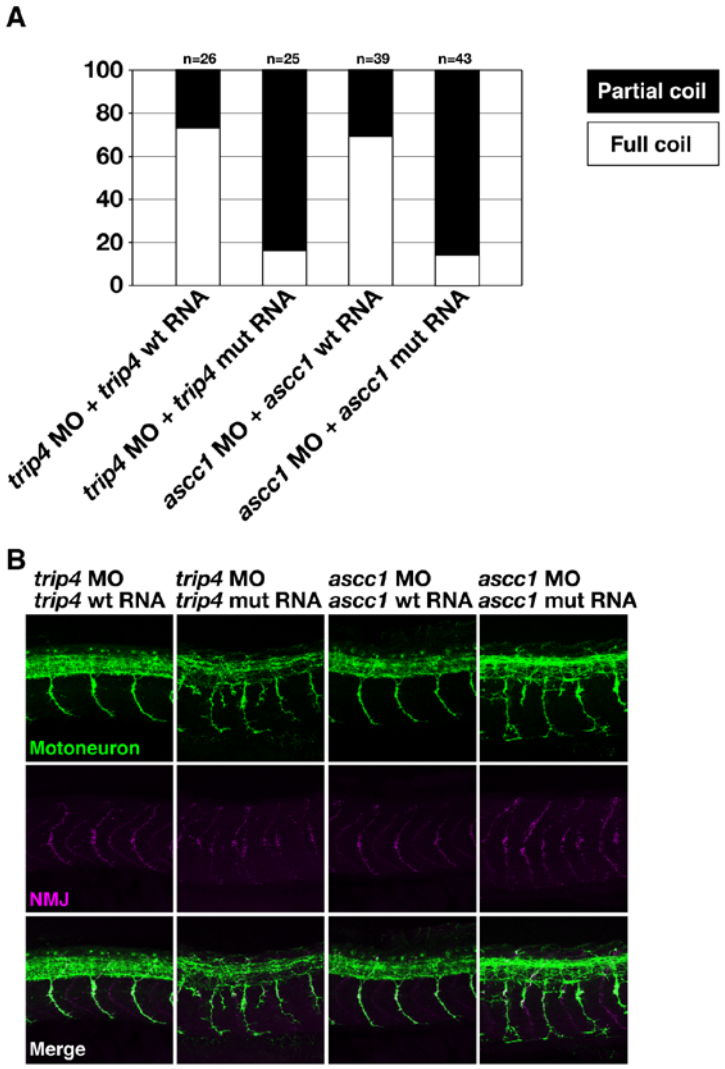

Figure S11. **Rescue of MO-knockdown with wildtype and mutant mRNAs.** Simultaneous injection of morpholinos and rescue mRNA into zebrafish larvae rescues **(A)** the clinical phenotype ("coiling" behavior) and **(B)** the morphological abnormalities of the α-motoneuron projections only if wildtype mRNA is injected and not by injection of mRNA carrying the zebrafish equivalents of the patient mutations.

Expression of SRF responsive genes after serum challenge

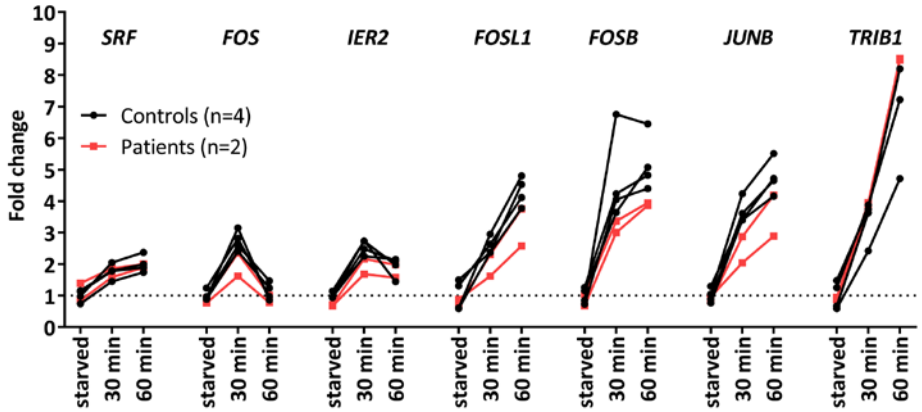

Figure S12. **Expression of known SRF responsive target genes after serum challenge.** Human skin fibroblasts were grown in DMEM + 15% FBS, then serum starved for 24 hours and re-challenged with 15% FBS for 30 and 60 minutes. The lines depict the fold change of gene expression from baseline (serum starvation). The red lines depict the patients, the black lines the controls. There was no significant and persistent difference in the response of the SRF downstream target genes.

Subcellular location of the ASC-1 complex and of the CSRP1 protein

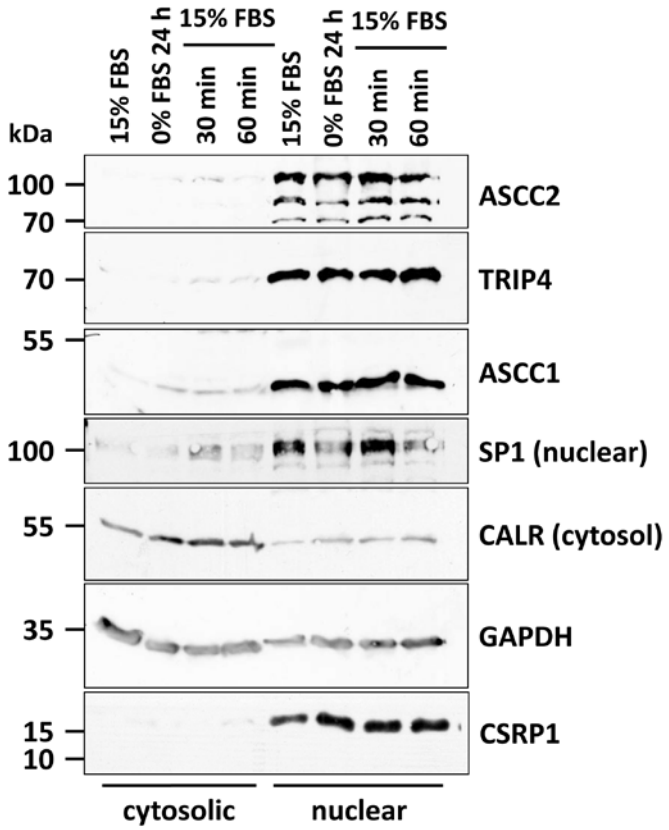

Figure S13. **Subcellular localization of the ASC-1 complex and of the CSRP1 protein after serum starvation and challenge.** The members of the ASC-1 complex TRIP4, ASCC1, and ASCC2 as well as the CSRP1 protein remain in the nucleus independently of the status of serum depletion or challenge of fibroblasts. As control for the subcellular fractionation, transcription factor SP1, a nuclear maker protein, is enriched in the nuclear fraction and the Calreticulin protein (CALR), a marker protein for the endoplasmatic reticulum (ER) is depleted in the nuclear fraction.

Multiple species alignment of TRIP4 and ASCC1 amino acid sequences

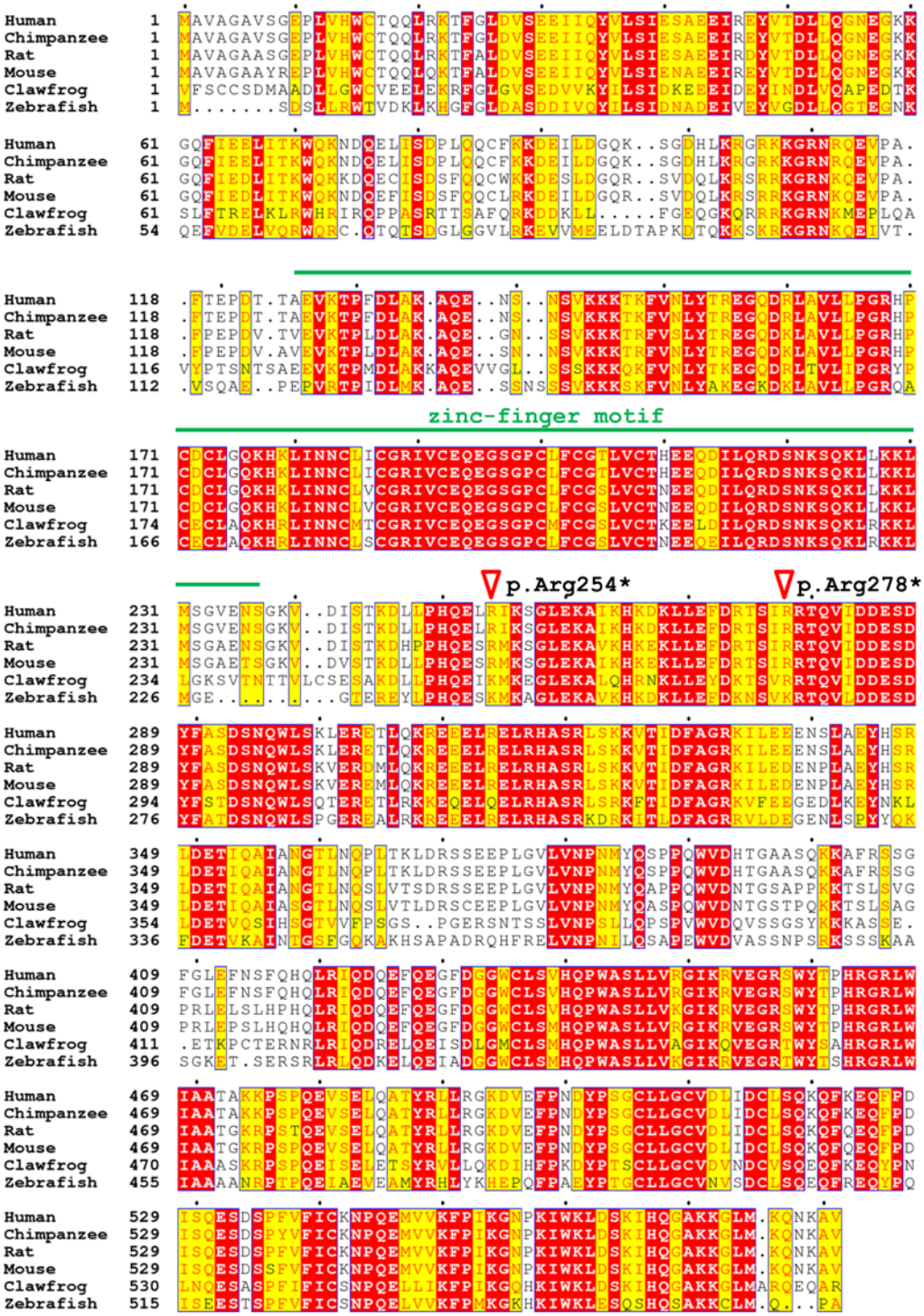

Figure S14. **Multiple species alignment of TRIP4** Red boxes depict identical, yellow boxes similar amino acids. The zinc-finger motif (aa125-237) is depicted by a green line. The positions of the two nonsense mutations are depicted by a red triangle. The Ensembl accession number for the amino acid sequences are: Human [ENSP00000261884], Chimpanzee [ENSPTRP00000012241], Rat [ENSRNOP00000021863], Mouse [ENSMUSP00000112385], Clawfrog [ENSXETP00000023326], Zebrafish [ENSDARP00000107782]

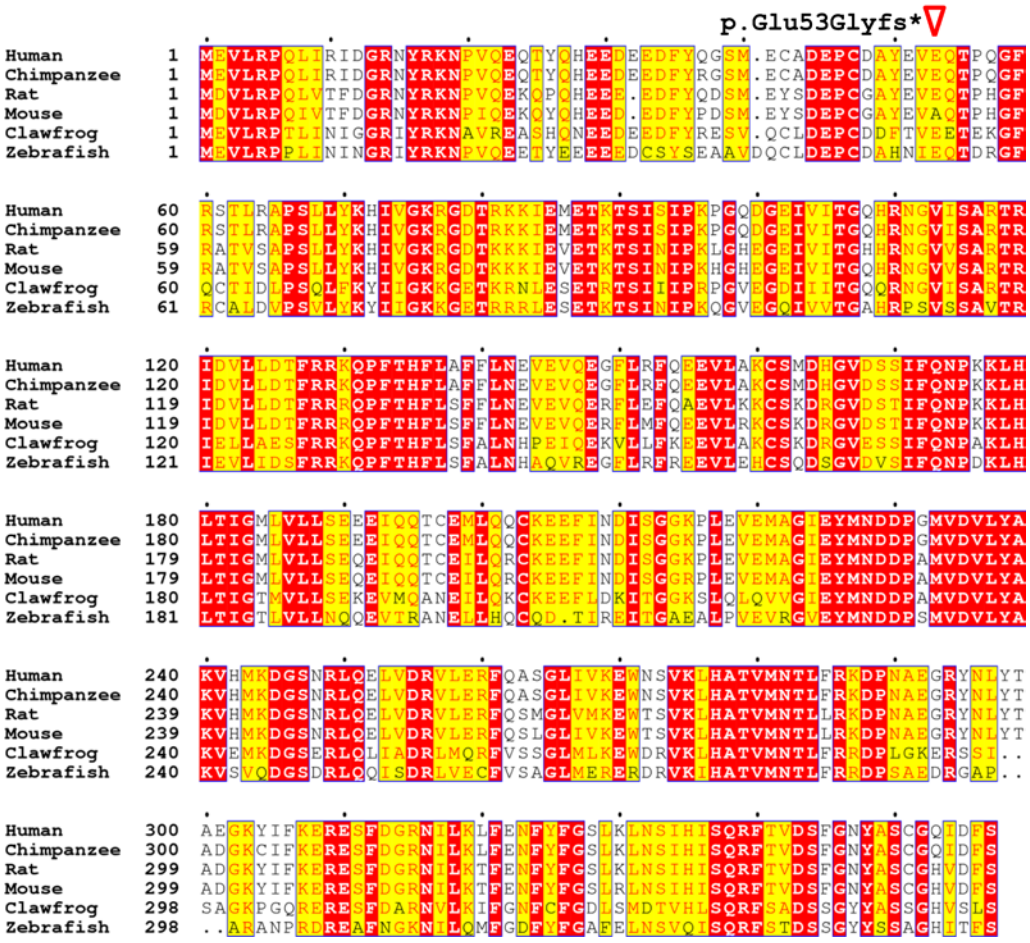

Figure S15. **Multiple species alignment of ASCC1** Red boxes depict identical, yellow boxes similar amino acids. The position of the frameshift mutation is depicted by a red triangle. The Ensembl/GenBank accession number for the amino acid sequences are: Human [ENSP00000320810], Chimpanzee [ENSPTRP00000004528], Rat [ENSRNOP00000000701], Mouse [ENSMUSP00000052351], Clawfrog [ENSXETP00000013525], Zebrafish [NP_001017610]. The multiple amino acid sequence alignment was performed with T-Coffee and the coloring /printout with ESPript.[1]

Co-immunoprecipitation with antibodies against three subunits of the ASC-1 complex

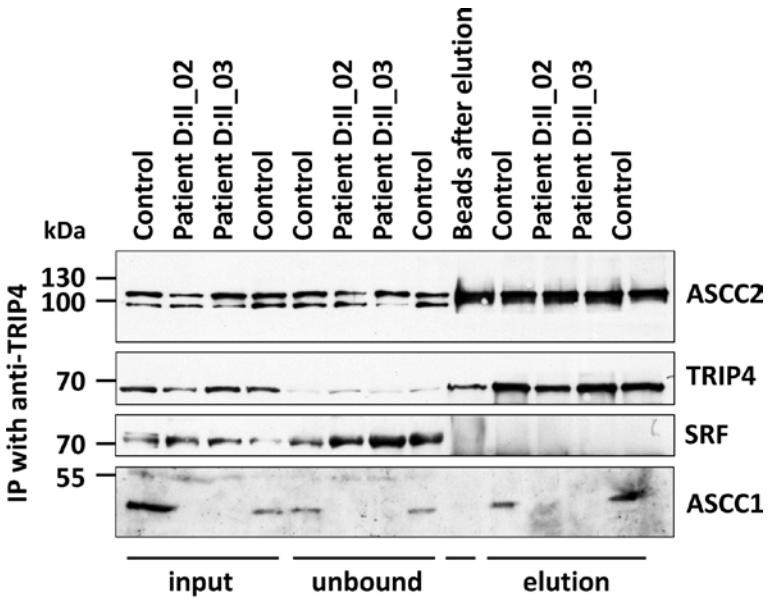

Figure S16. **Immunoprecipitation with an anti-TRIP4 antibody.** Co-precipitation with TRIP4 can be seen for ASCC1, and ASCC2. ASCC1 is only seen controls, but not in both patients. Hence, even in the absence of the ASCC1 subunit the remaining ASC-1 protein complex seems to be formed. SRF is not co-precipitated TRIP4 (or the ASC-1 complex) and can only be detected in the unbound flow-through.

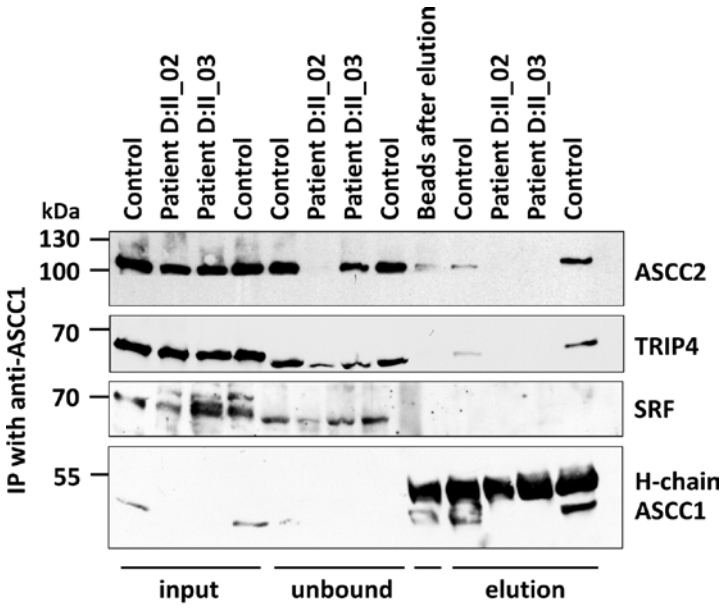

Figure S17. **Immunoprecipitation with an anti-ASCC1 antibody.** Co-precipitation with ASCC1 can be seen for TRIP4 and ASCC2 only in the controls, not in the patients. SRF is not co-precipitated ASCC1 (or the ASC-1 complex) and can only be detected in the unbound flow-through.

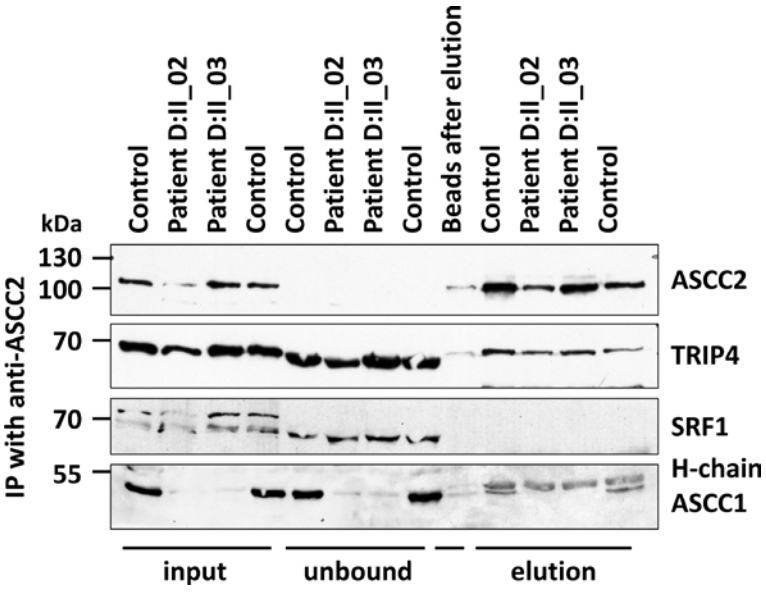

Figure S18. **Immunoprecipitation with an anti-ASCC2 antibody. (A)** Co-precipitation with ASSC2 can be seen for TRIP4 and ASCC1 only in the controls, not in the patients. SRF is not co-precipitated ASCC2 (or the ASC-1 complex) and can only be detected in the unbound flow-through.

HCD spectra of peptides from interacting proteins

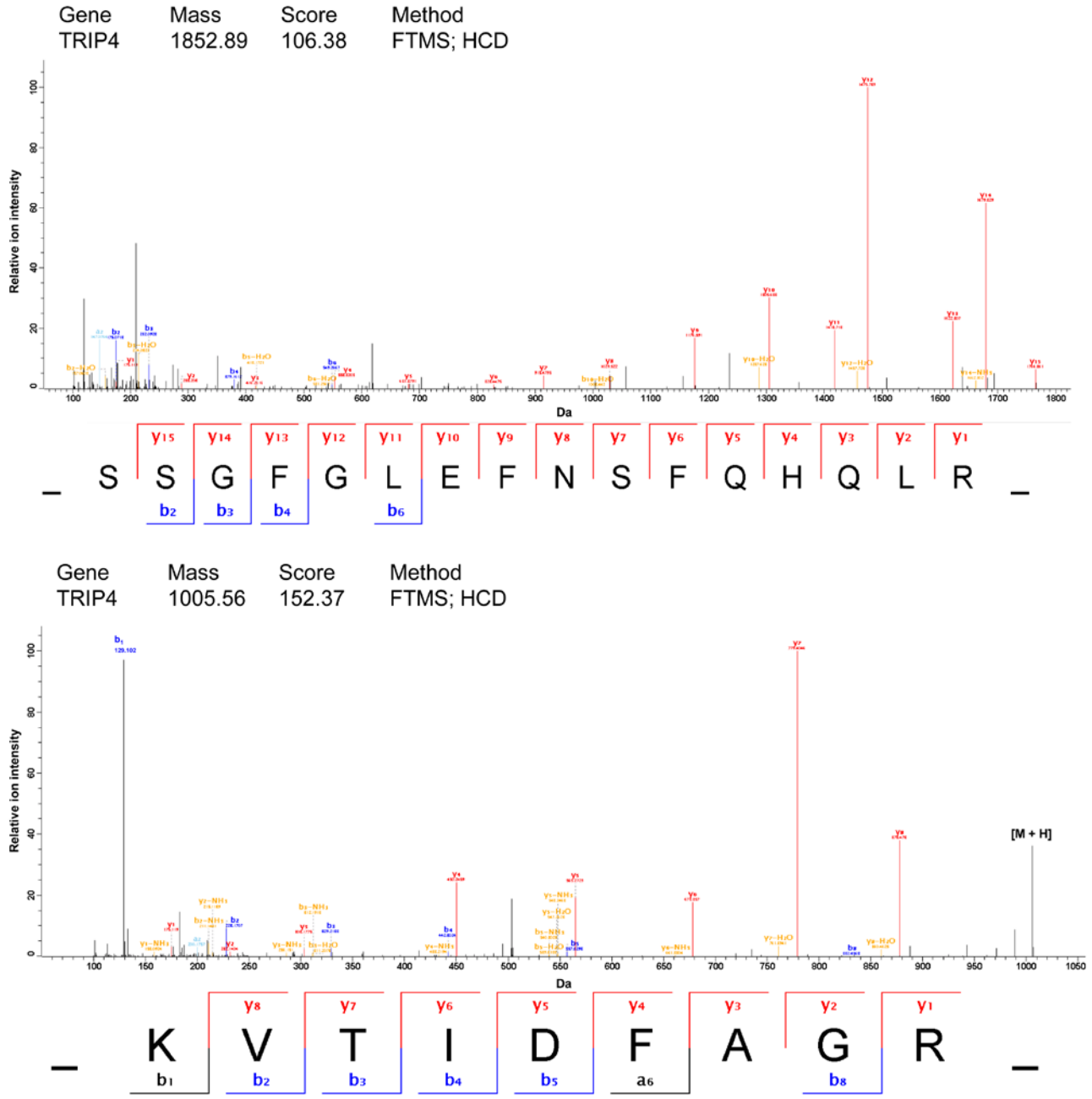

Figure S19. **MS spectra of two identified TRIP4 peptides.** The b- and y- ion series of the Higher-energy collisional dissociation (HCD) spectrum.

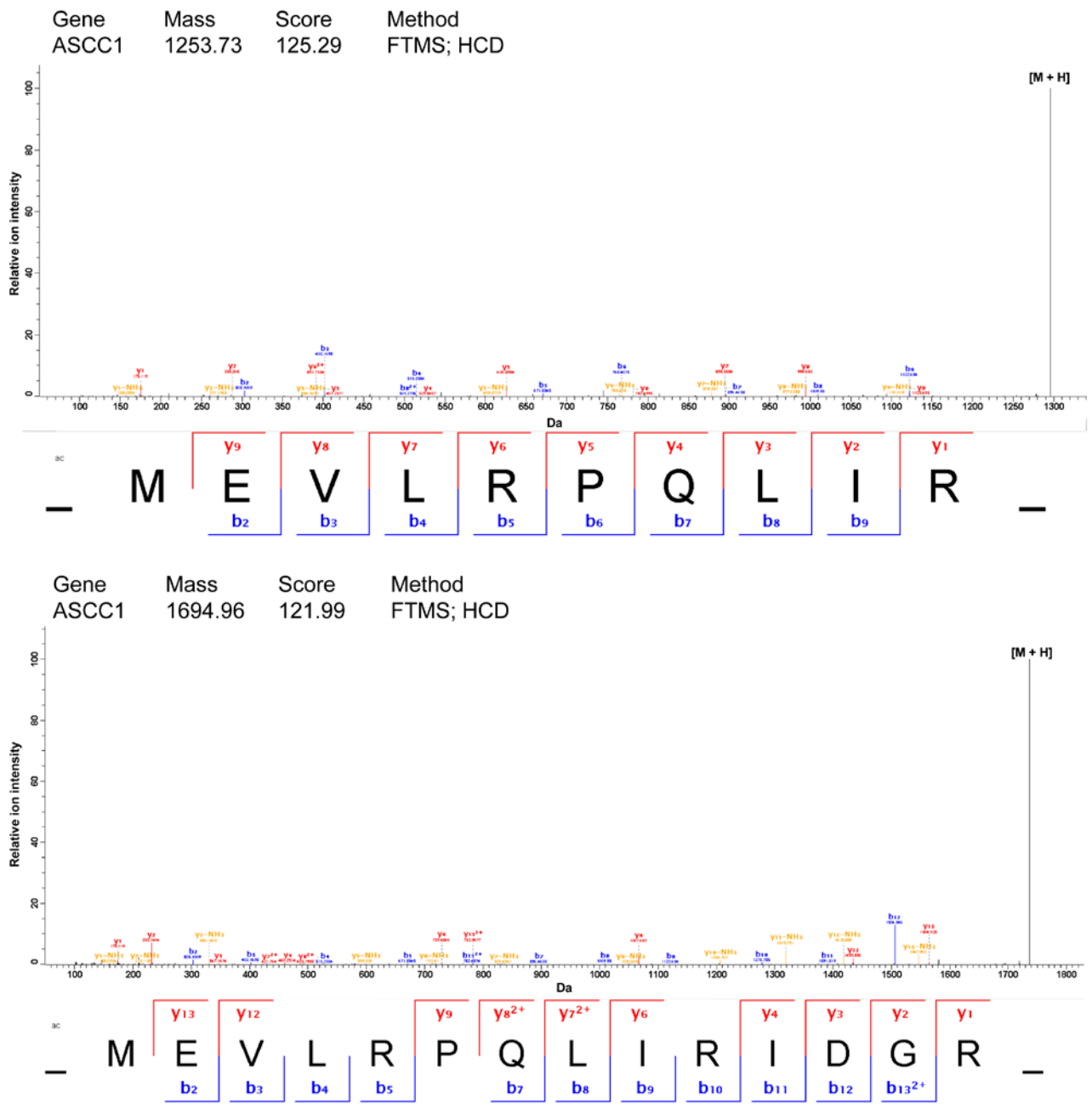

Figure S20. **MS spectra of two identified ASCC1 peptides.** The b- and y- ion series of the Higher-energy collisional dissociation (HCD) spectrum.

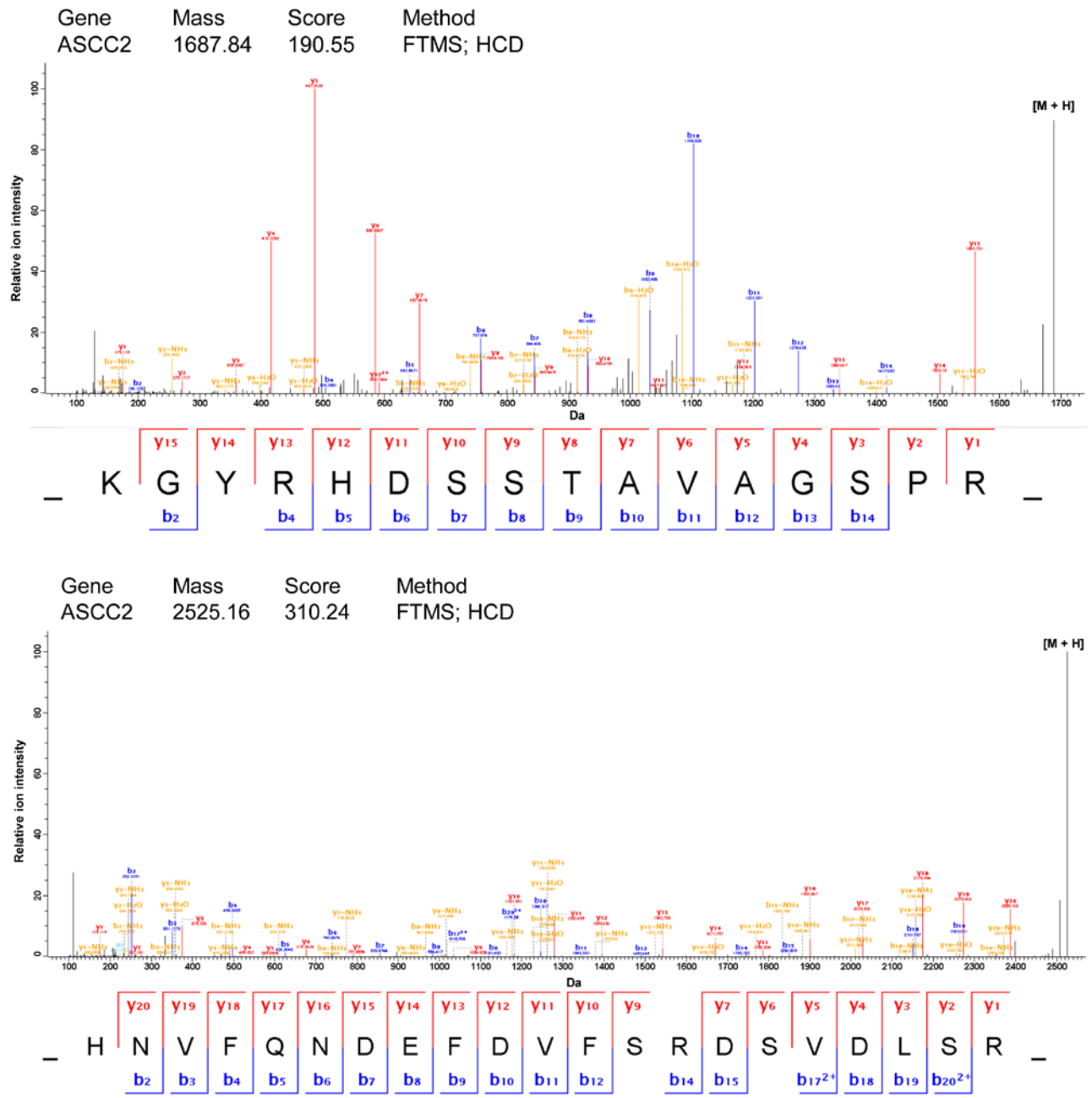

Figure S21. **MS spectra of two identified ASCC2 peptides.** The b- and y- ion series of the Higher-energy collisional dissociation (HCD) spectrum.

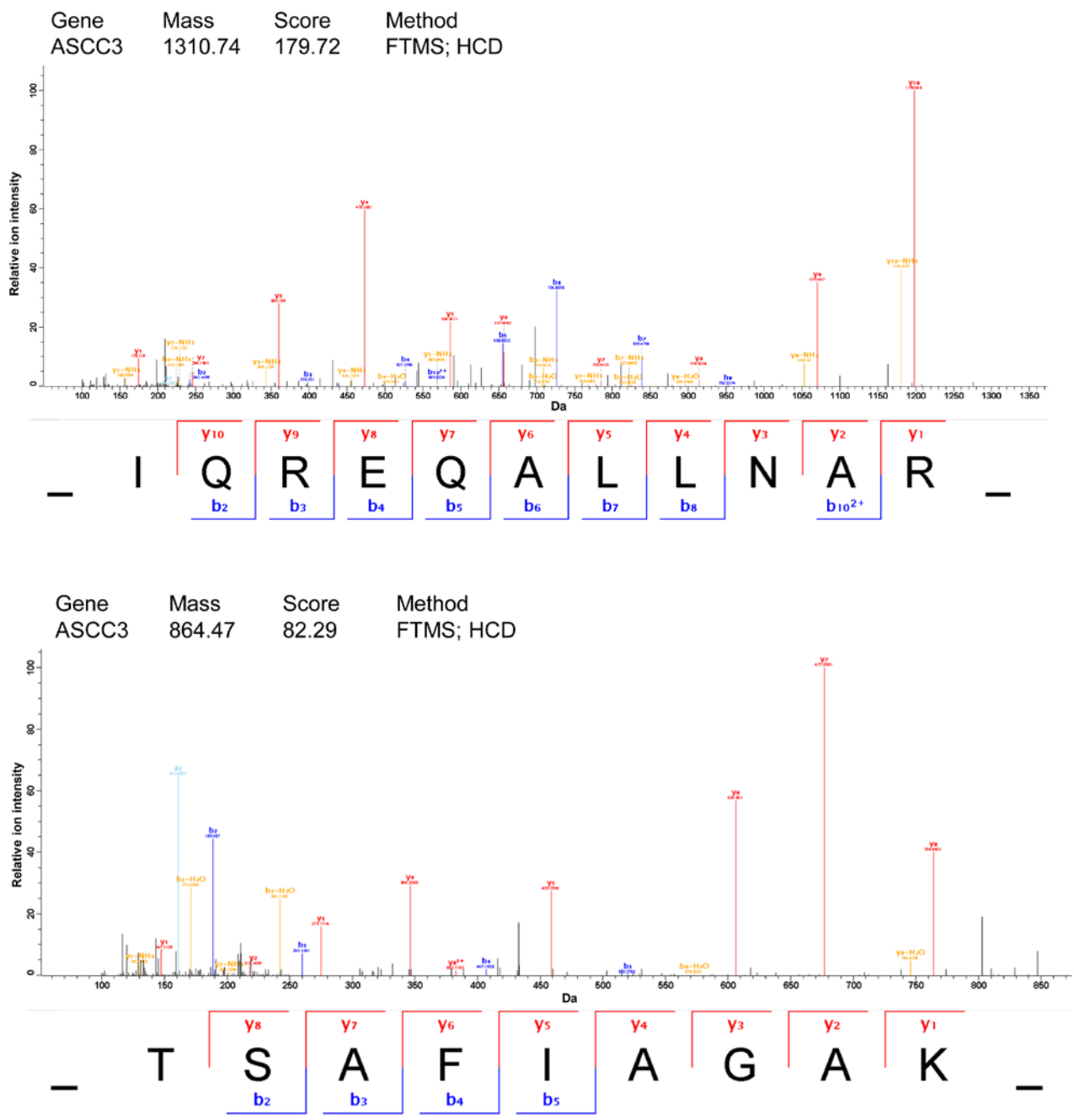

Figure S22. **MS spectra of two identified ASCC3 peptides.** The b- and y- ion series of the Higher-energy collisional dissociation (HCD) spectrum.

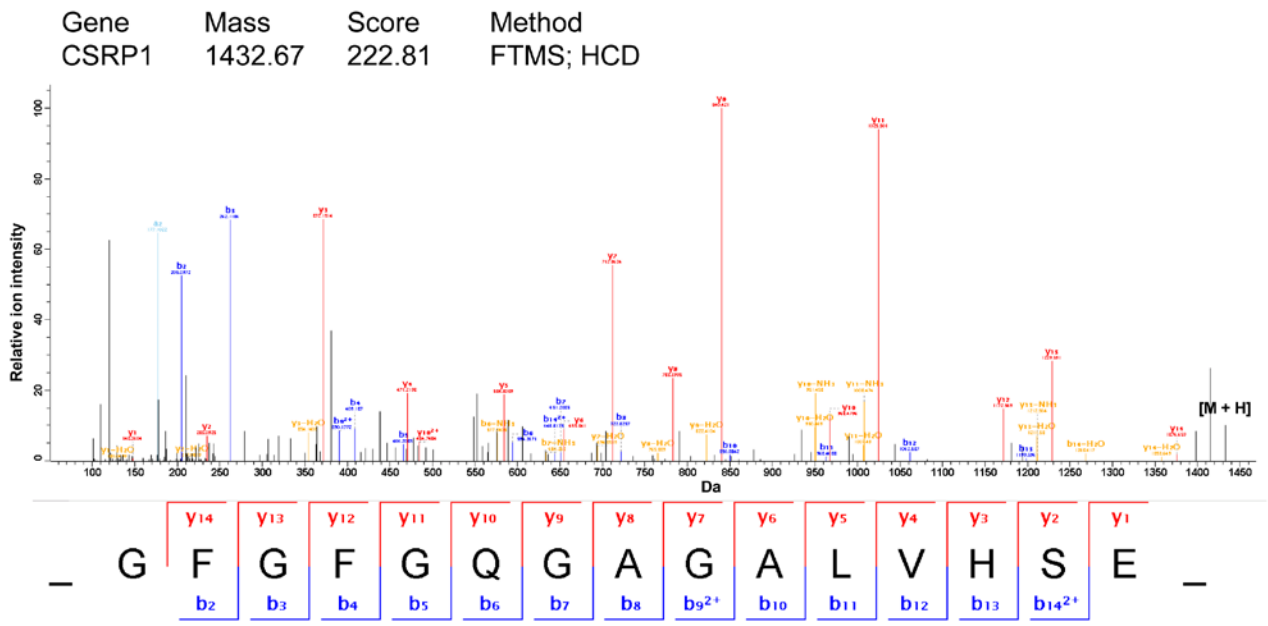

Figure S23. **MS spectrum of one identified CSRP1 peptide.** The b- and y- ion series of the Higher-energy collisional dissociation (HCD) spectrum.

Morphometric analysis of the sural nerve

Table S1. **Fiber density of myelinated fibers in patients and control**

Patient	Median	10th percentile	90th percentile
Control	22,059 mm^2	18,971 mm^2	25,111 mm^2
B:II_05 (*TRIP4*)	22,752 mm^2	21,781 mm^2	23,169 mm^2
D:II_02 (*ASCC1*)	21,781 mm^2	16,509 mm^2	28,857 mm^2

Coverage details of the exome sequencing

Table S2. **Coverage details of three WES datasets**

Individual	Mean coverage [fold]	Coverage per base of captured exons			100 bp paired-end fragments [n]
		>3x [%]	>10x [%]	>20x [%]	
B.II_01	175.99	99.8	99.4	98.7	77.3 Mio
D.II_02	112.91	99.5	98.7	97.0	53.2 Mio
D.II_03	230.12	99.8	99.5	98.9	106.1 Mio

Quantification of morpholino injection into zebrafish

Table S3. **Quantification of the "coiling" behavior of morphants and controls**

Morpholino [amount injected]		**"partial coil"/total number of examined embryos (p-value in comparison to *bactin* MO injection; χ^2-test)**	**Affected embryos [%]**
Control [5 ng]		0/43 (p<0.001)	0
trip4 MO [5 ng]		49/62 (p<0.001)	79
ascc1 MO [5 ng]		46/55 (p<0.001)	84
Morpholino [amount injected]	**Primer set**	**Specific/bactin RT-PCR band density [mean±SD; t-test]**	**N**
trip4 MO [5 ng]	*trip4*	0.15±0.09 (p<0.01)	4
trip4 MO [5 ng]	*ascc1*	0.92±0.07 (p>0.05)	4
ascc1 MO [5 ng]	*trip4*	1.03±0.31 (p>0.80)	4
ascc1 MO [5 ng]	*ascc1*	0.17±0.09 (p<0.01)	4

Table S4. **Quantification of the "coiling" behavior using an alternative morpholino**

Morpholino [amount injected]		**"partial coil"/total number of examined embryos (p-value in comparison to *bactin* MO injection; χ^2-test)**	**Affected embryos [%]**
Control [5 ng]		0 /19 (p<0.001)	0
trip4 MO2 [5 ng]		24/28 (p<0.001)	86
ascc1 MO2 [5 ng]		35/43 (p<0.001)	81
Morpholino [amount injected]	**Primer set**	**Specific/bactin RT-PCR band density [mean±SD; t-test]**	**N**
trip4 MO2 [5 ng]	*trip4*	0.19±0.11 (p<0.001)	4
trip4 MO2 [5 ng]	*ascc1*	1.00±0.09 (p>0.9)	4
ascc1 MO2 [5 ng]	*trip4*	0.92±0.09 (p>0.15)	4
ascc1 MO2 [5 ng]	*ascc1*	0.14±0.10 (p<0.001)	4

Table S5. **Quantification of the density of neuromuscular junctions**

Morpholino	**Amount injected [ng]**	**Cumulative relative density of the neuromuscular junction in comparison to CTRL MO [± SD]**
CTRL MO	5	1.00±0.26 (n=4)
ascc1 MO	5	0.61±0.12 (n=4, p<0.05)
trip4 MO	5	0.56±0.18 (n=4, p<0.05)

Quantification of gene expression in patient and control fibroblasts

Table S6. **Differentially regulated genes in *ASCC1* mutant versus control skin fibroblasts**
(The PubMed link can be directly clicked and connects to the PubMed abstract of the cited article)

Gene symbol (HGNC)	Fold change	FDR (BH)	Gene name	Gene Ontology (GO) annotation	Direct link to PubMed
Genes in nervous system development (DOWN-REGULATED)					
SERPINF1	**-5.7**	0.0045	Serpin peptidase inhibitor, clade F (alpha-2 antiplasmin, pigment epithelium derived factor), member 1	positive regulation of neuron projection development	PMID:23825416
				neuronal cell body	PMID:10411342
				negative regulation of neuron death	PMID:22410737
				positive regulator of neurogenesis	PMID:8226833
GSTM3	**-2.1**	0.0045	Glutathione S-transferase mu 3 (brain)	establishment of blood-nerve barrier	PMID:2345169
DAB1	**-6.4**	0.0045	Dab, reelin signal transducer, homolog 1 (Drosophila)	lateral motor column neuron migration	PMID:20711475
				positive regulation of neuron differentiation	PMID:18848628
				neuron migration	PMID:15703280, PMID:15091337, PMID:11226314, PMID:12882964, PMID:8875886
				neuron projection	PMID:14961563
				neuronal cell body	PMID:14961563
LAMA4	**-2.8**	0.0045	Laminin, alpha 4	muscle attachment	PMID:22859503
FHOD3	**-2.1**	0.0045	Formin homology 2 domain containing 3	sarcomere organization	PMID:19706596, PMID:22509354
CRLF1	**-2.2**	0.0045	Cytokine receptor-like factor 1	negative regulation of neuron apoptotic process	PMID:10966616
				negative regulation of motor neuron apoptotic process	PMID:14523086
SEMA3D	**-2.3**	0.0045	Semaphorin 3D	axon guidance	PMID:15456815, PMID:17251263
				peripheral nervous system development	PMID:16280593
				retinal ganglion cell axon guidance	PMID:14724229, PMID:16467361
				Neural crest development	PMID:16971468
				regulation of axon extension	PMID:16280593
				neural crest cell differentiation	PMID:16860789, PMID:16971468

SEMA3A	**-5.1**	0.0045	Semaphorin 3A	retinal ganglion cell axon guidance	PMID:16467361, PMID:14724229
				neural crest cell development	PMID:16971468
				regulation of axon extension	PMID:16280593
				pathway involved in axon guidance	PMID:18804103
				axogenesis involved in innervation	PMID:22790009
PPAP2B	**-1.9**	0.0045	Phosphatidic acid phosphatase type 2B	Bergmann glial cell differentiation	PMID:21319224
				ossification	PMID:12933688
				response to vitamin D	PMID:11702003
CRABP2	**-1.6**	0.0078	Cellular retinoic acid binding protein 2	embryonic forelimb morphogenesis	PMID:7720575
				hindbrain morphogenesis	PMID:22619388
				positive regulation of collateral sprouting	PMID:18052984
FZD4	**-2.1**	0.0045	Frizzled class receptor 4	cerebellum vasculature morphogenesis	PMID:15035989, PMID:12230512
ASPA	**-2.7**	0.0078	Aspartoacylase	positive regulation of oligodendrocyte differentiation	PMID:16634055
NOV	**-2.6**	0.0078	Nephroblastoma overexpressed	axon development	PMID:19286457
				neuronal cell development	PMID:19286457
				dendrite formation	PMID:19286457
Genes in nervous system development (UP-REGULATED)					
HAPLN1	**+6.7**	0.0045	Hyaluronan and proteoglycan link protein	Suppression of neuronal plasticity	PMID:20566484
				Memory function	PMID:23595763
				Extracellular matrix	PMID:23595763
EDIL3	**+3.1**	0.0045	EGF-like repeats and discoidin I-like domains 3	Neural plate development	PMID:20823067
NTN4	**+3.1**	0.0045	Netrin 4	Neuron remodeling	PMID:11038171
ITGA	**+1.7**	0.0045	Integrin alpha-3	Neuron migration	PMID:15091337
				Excitatory synapse	PMID:23595732
				Regulation of neuron projection development	PMID:2223092
CDH13	**+2.0**	0.0045	Cadherin-13	Negative regulation of neuron projection	PMID:10737605
				Negative regulation of cell proliferation	PMID:10737605

Gene symbol (HGNC)	Fold change	FDR (BH)	Gene name	Gene Ontology (GO) annotation	Direct link to PubMed
Genes in bone development (DOWN-REGULATED)					
TNFRSF11B	**-4.8**	0.0045	Tumor necrosis factor receptor superfamily, member 11b	negative regulation of odontogenesis of dentin-containing tooth	PMID:16283633 PMID:14981127
				negative regulation of bone resorption	PMID:11839361 PMID:16912914
				skeletal system development	PMID:9108485
FAM20A	**-1.9**	0.0045	Family with sequence similarity 20, member A	tooth eruption	PMID:23434854 PMID:23468644 PMID:23697977
				calcium ion homeostasis	PMID:23434854
RASSF2	**-2.5**	0.0078	Ras association (RalGDS/AF-6) domain family member 2	bone remodeling	PMID:22227519
				ossification	PMID:22227519
				regulation of osteoblast differentiation	PMID:22227519
				regulation of osteoclast differentiation	PMID:22227519
				skeletal system development	PMID:22227519
TSHZ2	**-2.2**	0.0045	Teashirt zinc finger homeobox 2	embryonic cranial skeleton morphogenesis	PMID:23559552
STC1	**-3.0**	0.0078	Stanniocalcin 1	positive regulation of calcium ion import	PMID:17032941
DPT	**-2.5**	0.0045	Dermatopontin	collagen fibril organization	PMID:16877395

Mass spectrometric analysis of peptides from immunoprecipitations

Table S7. **Mass spectrometric analysis of peptides from immunoprecipitations (TableS7.xlsx)**

Immunoprecipitated samples were boiled at 95°C for 5 min, reduced in 50 mM DTT and alkylated with a final concentration of 5.5 mM chloroacetamide for 30 min. Proteins were digested by 250 ng of trypsin overnight at 37°C and desalted with C18 columns. Each sample fraction was dissolved in 2 µL of 5% ACN and 2% FA for subsequent MS analysis. LC–MS/MS was carried out by nanoflow reverse-phase liquid chromatography (Dionex Ultimate 3000, Thermo Scientific; Waltham, MA) coupled online to a Q-Exactive Plus Orbitrap mass spectrometer (Thermo Scientific). Briefly, LC separation was performed using a PicoFrit analytical column (75 µm ID × 25 cm long, 15 µm Tip ID (New Objectives, Woburn, MA)) in -house packed with 3 µm C18 resin (Reprosil-AQ Pur, Dr. Maisch, Germany). Peptides were eluted using a gradient from 3.8 to 98% solvent B over 46 min at a flow rate of 300 nL/min (solvent A: 0.1% formic acid in water; solvent B: 80% acetonitrile and 0.08% formic acid). Three kilovolts were applied for nanoelectrospray generation. A cycle of one full FT scan mass spectrum (300–1700 m/z, resolution of 35000 at m/z 200) was followed by 12 data-dependent MS/MS scans with a normalized collision energy of 25 eV. Raw MS data were processed with MaxQuant software (version 1.5.0.0) and searched against the human proteome database UniProtKB with 88,717 entries, released 2014-11. A false discovery rate (FDR) of 0.01 for proteins and peptides and a minimum peptide length of 7 amino acids were required. A maximum of two missed cleavages was allowed for the tryptic digest. Cysteine carbamidomethylation was set as fixed modification, whereas N-terminal protein acetylation and methionine oxidation were set as variable modifications.

Oligonucleotides used for sequencing, cloning, in vitro mutagenesis and morpholino mediated knockdown

Table S8. **Oligonucleotides used for molecular genetics experiments**

Gene	Exon	Forward	Reverse	Product size [bp]
Sequencing of genomic DNA				
ASCC1	Ex 3	5-CCCAATTCAGACCTGCATAA-3	5-TTGATCCTACAATACACAGGACA-3	296
ASCC1	Ex 4	5-AGCGGTTGACAGCTGAGG-3	5-TCAAGCACTGCAATAAGTATGGA-3	275
ASCC1	Ex 5	5-TCTCTTGTCACAAAGGATTTAAACA-3	5-CCCATAGCTAGAACCCCACA-3	299
ASCC1	Ex 6	5-TCAGAACTGCTTTAGCTCCTCA-3	5-TTGGTGGGGGAAGAAGTTTA-3	390
ASCC1	Ex 7	5-TGGGCTGAGTTTCTTGTTTT-3	5-CTGAGAATTACTCACATACCAAAAAG-3	249
ASCC1	Ex 8	5-TTTTGAAATTAGAAGGGCAATTAGA-3	5-TCAAAGAAAAGGAATCAAAATGAA-3	381
ASCC1	Ex 9	5-GCAGGGCTTTGTATGGTGAT-3	5-TTGCCCACCTCTACTATGCTC-3	395
ASCC1	Ex 10	5-TCATTATGCCACTTTCCAGGT-3	5-TGAAGAAATATACGGAGAACTACTTG-3	298
ASCC1	Ex 11	5-GGGATTGTTGTGGTTTGGTG-3	5-CCCTGCTTGGCAATTAAAAC-3	300
Sequencing of genomic DNA				
TRIP4	Ex 1	5-GGGATCTGCACTGGAGGC-3	5-GCACATCCCAGAGCTCCTT-3	289
TRIP4	Ex 2	5-CTCTGTTAAGATTACTGAGAAACAGTG-3	5-AGCCTGCCCACTTACCAATA-3	291
TRIP4	Ex 3	5-TTCACCAGGAATCCTCTTATCAA-3	5-TCACTTCCTCTTCTCCAATAGTCA-3	248
TRIP4	Ex 4	5-GGAGCATTTTCTCCCTTGAC-3	5-AGATCTGACTGGCTCTGCGT-3	352
TRIP4	Ex 5	5-GCAATATAATTTAACTGTTGGATCAC-3	5-ACAAGGTACCCATCATCCCA-3	178
TRIP4	Ex 6	5-TTGTTCTTTGTTGCACACTGG-3	5-ATGGCCAGAATCTGTGGACT-3	267
TRIP4	Ex 7	5-AATCGGTCCTTATTTGTCAACAG-3	5-GACCCTTTCTAGTGCTGCTCA-3	298
TRIP4	Ex 8	5-TGTTGGTGGTAAGCATTCTGAG-3	5-AAATTGGGGCCAAACTTCTT-3	244
TRIP4	Ex 9	5-ACCTACCCCAGATTCTTGCC-3	5-TCTAAGATCTTCCACTGCCCA-3	285
TRIP4	Ex 10	5-TGGGATATTCCAGGAAACTAGA-3	5-AACGTCAATGACTTCTCTCCA-3	241
TRIP4	Ex 11	5-TCCTGAGTTCCAAGATCACAAA-3	5-ATGGCGAAACCCTGTCTCTA-3	199
TRIP4	Ex 12	5-GCTTGTCCCAACTATCCTGAA-3	5-TCCCCATTCCTTACTACTGCAC-3	204
TRIP4	Ex 13	5-TAACCAGAAGACCTGGGAGG-3	5-TTTCCAACTTGGTCCAATCTC-3	445

Tailed primers for the cloning of the in-situ hybridization probes				
Trip4	*Not*I-*Sal*I	5-GGAGGAGCGGCCGCCGTACCGGGAGCCGCTAGTA-3 (*Not*I site underlined)	5-GGAGGAGTCGACCTTCTGGCCCAGGCAATCAC-3 (*Sal*I site underlined)	512
Ascc1	*Not*I-*Sal*I	5-GGAGGAGCGGCCGCTCCAGGAGGAGGTGCTGAGG-3 (*Not*I site underlined)	5-GGAGGAGTCGACTCCAAAGCTGTCCACCGTGA-3 (*Sal*I site underlined)	581
Two different sets of morpholinos used for *trip4* and *ascc1* knockdown				
trip4	*MO*	5-ATTGGTGCACACCTGAATGATGTGC-3		
ascc1	*MO*	5-TGCACCTGTGACCACTGAGAGAAC-3		
trip4	*MO2*	5-AGTGCGAGCTCACCAGACTGCCGCA-3		
ascc1	*MO2*	5-ATACACTGACTTGTAAAGCACACTG-3		
bactin	*MO*	5-CCTCTTACCTCAGTTACAATTTATA-3		
Primers used for RT-PCR quantification of *trip4*, *ascc1*, and control (*bactin*) mRNA abundance after MO and MO2-knockdown				
trip4	*Ex4-5*	5-CTCCCATTGACTTAATGAAGGCAC-3	5-GGTTCCCTCTCCCATCAG-3	
ascc1	*Ex2-4*	5-GCAGCAGTGGATCAGTGTC-3	5-CCCTGAGTCCTGTGAGC-3	
bactin	*Ex1-2*	5-CCTTCCTTCCTGGGTATGG-3	5-GGGGGAGCAATGATCTTGATC-3	
Primers used for cloning of full length *trip4* and *ascc1* constructs and for site directed mutagenesis				
trip4	*cloning*	5-GGAATTCGCCGCCACC**ATG**AGCGATTCTTTGCTTCGCT GGAC-3 (start codon underlined)	5-GCTCGAG**TCA**CGCTGGCTGCATTAAACACTT CTTG-3 (stop codon underlined)	1784
trip4	p.K265*	5-GAATTTGACAAGAACAGTGTT**T**AGAGAACACAAGTCT TG-3 (mutant residue underlined)	5-CAAGACTTGTGTTCTCT**A**AACACTGTTCTTGT CAAATTC -3 (mutant residue underlined)	
ascc1	*cloning*	5-GAATCGATGCCGCCACC**ATG**GAGGTCTTACGGCCGCC-3 (start codon underlined)	5-GTCTAGA**TCA**TGAGAATGTGATGTGTCCGGCTG-3 (stop codon underlined)	1165
ascc1	*fs*	5-CGATGCTCATAACATAG**G**AGCAGACGGAC-3 (inserted nucleotides underlined)	5-GTCCGTCTGCT**C**CTATGTTATGAGCATCG-3 (inserted nucleotides underlined)	

Antibodies for immunostaining, immunoprecipitation, and Western blot

Table S9. **List of used antibodies**

AB against	Species	Raised in species	Company	Order number
TRIP4	Humans	Rabbit-pAB (IgG)	ATLAS	HPA016605
ASCC1	Humans	Goat-pAB (IgG)	Santa Cruz	sc-160156
ASCC2	Humans	Rabbit-pAB (IgG)	Sigma/Prestige	HPA001439
CSRP1	Humans	Rabbit-pAB (IgG)	Abcam	ab70010
CALR	Humans	Rabbit-mAB (IgG), clone EPR3924	Millipore	MABT145
SP1	Humans	Rabbit-pAB	Millipore	07-645
MHC_{fast}	Humans	Rabbit-mAB (IgG1)	Novocastra/Leica	Clone: WB-MHCf
MHC_{slow}	Humans	Rabbit-mAB	Novocastra/Leica	Clone: WB-MHCs
MHC_{neo}	Humans	Rabbit-mAB (IgG1)	Novocastra/Leica	Clone: WB-MHCn
MHC_{dev}	Humans	Rabbit-mAB (IgG1)	Novocastra/Leica	Clone: WB-MHCd
GAPDH	Humans	Mouse-mAB (IgG1)	Ambion/Applied Biosystems	AM4300, Clone: 6C5
β-Tubulin	Humans	Rabbit-pAB (IgG)	Abcam	ab6046
pan-Actin	Humans	Mouse-mAB (IgG1), clone C4	Chemicon international	MAB1501R
znp-1	Zebrafish	Mouse-mAB (IgG2a,κ)	DSHB	znp-1
		AlexaFluor594-α-Bungarotoxin	Life Technologies/Molecular Probes	B-13423
		Protein G Sepharose 4B	Life Technologies	101241